Title
The Molecular Mechanisms of Mechanosensitive Neural Stem Cell Differentiation

Author
Kang, Michael

Publication Date
2017

Peer reviewed|Thesis/dissertation

The Molecular Mechanisms of Mechanosensitive Neural Stem Cell Differentiation

By Michael Kang

A dissertation submitted in partial satisfaction of the requirements of the degree of

Joint Doctor of Philosophy

with University of California, San Francisco

in

Bioengineering

in the Graduate Division

of the

University of California, Berkeley

Committee in charge:

Professor David Schaffer, Chair

Professor Sanjay Kumar

Professor Tamara Alliston

Professor Daniela Kaufer

Professor Andrew Dillin

Fall 2017

Abstract

The Molecular Mechanisms of Mechanosensitive Neural Stem Cell Differentiation

By

Michael Kang

Joint Doctor of Philosophy in Bioengineering

with University of California, San Francisco

University of California, Berkeley

Professor Sanjay Kumar, Chair

Until recently, adult mammals were not believed to maintain active neurogenesis into adulthood, and brains were thought to be fully formed and most-mitotic by the end of adolescence. However, it has recently been appreciated that continuous neurogenesis in mammals occurs in the subventricular and subgranular zones of the brain, and the ongoing process of neurogenesis has ramifications for mammalian learning, memory formation, and diseases such as Alzheimer's. They also serve as a potential reservoir for transplantation or stimulation therapies, where stem cells can repopulate and repair areas of the central nervous system damaged by disease or injury. However, in order to harness the potential of these cells and to understand the processes of learning and memory in mammals, we must first understand the deep molecular identities and pathways that govern stem cell fate specification and behavior. A growing body of literature has identified many factors that influence neural stem cell (NSC) differentiation, which includes soluble signals such as sonic hedgehog or VEGF or cell-cell signals such as Notch and ephrins. However, in addition to biochemical cues, mechanical properties of the stem cell niche such as substrate stiffness have also been found to contribute strongly to NSC fate specification.

A panel of studies were undertaken in order to determine the biological relevance of substrate stffness in NSC differentiation. We used atomic force microscopy to probe the natural stiffness variations and heterogeneities in the brain matrix, and then used these measurements to guide the synthesis of a dynamic, mechanically tunable hydrogel that allows for dynamic control of substrate stiffness. With this study, we identify a candidate molecular, YAP, that transduces information about extracellular elastic modulus to fate specification pathways within the cell – specifically, β-catenin. We then expand our model into a three-dimensional platform, and identify another signaling pathway critical for neurogenesis – CD44, a hyaluronan receptor molecule.

These discoveries improve our understanding of basic NSC mechanobiology, and reveal new target pathways for modulation in generating *in vitro* culture platforms or engineering NSCs for transplantation or stimulation therapies.

Acknowledgements

I am deeply grateful to the many people who have lent their technical expertise, scientific perspective, and emotional support while conducting the work presented in this dissertation – without them, none of this would have been possible.

I would like to thank my graduate advisors, Professors Sanjay Kumar and David Schaffer. I've been so fortunate to have the expertise, guidance, and wisdom of two leaders in the field, but also to have the support and understanding of two empathetic, invested, and caring mentors. I've learned so much from them, and both Sanjay and Dave remain my role models for professionalism, respect, and scientific excellence. Thank you to both of you – for the opportunities, for understanding, and for helping me to grow and learn as a researcher, hard lessons and all.

I would also like to thank my larger than typical (and larger than life) dissertation and qualifying exam committees – Professors Mohammad Mofrad, Tamara Alliston, Daniel Fletcher, Andrew Dillin, and Daniela Kaufer. Your insight, guidance, and difficult questions have made such a positive, tremendous difference in the path this research has taken, and I'm so grateful for their respective insights.

I'd like to thank my outside collaborators as well – Kevin Tharpe, for his contagious scientific energy and enthusiasm, and his mentor, Andreas Stahl. Tomas Luque, whom I worked with on the brain mapping project, for being a great friend and exceptionally supportive colleague.

I've had the good luck to have two labs to thank for helping me every day, and I apologize to anyone I am unable to name personally here – if I did, this section would be longer than my dissertation. First, I'd like to thank our past alumni who took me in and helped me find a home in Stanley Hall. Sebastian Rammensee, my collaborator on NSC work and first mentor, and Katerina Georgiou, who I peppered daily with questions, and Badri Ananthanarayanan and Jess Pei, who helped me learn a lot more chemistry than I ever thought I'd want to. I'd like to thank my visiting scholars as well – Dennis Huang and Jieung Baek, who made great scientific advances and always kept me on my toes learning how to be a better mentor. In particular I'd also like to thank Kayla Wolf, who, despite being a younger graduate student in the lab, is probably the person I've learned the most from in my last couple of years. I owe great personal thanks to Elena Kassianidou and Yushan Kim as well, for their scientific insight, great humor and attitude in the lab, and rides home from Stanley and a chance to pet Casper and Elba, respectively. I want to thank the NSC group as well – particularly, Phil Kang, my longtime NSC partner in crime, in addition to Andrew Bremer, Olivia Scheideler, Nicole Repina, Riya Muckom, and Paola Lopez for all the compared notes and "borrowed" laminin plates over the years. In particular I'd also like to thank Alyssa Rosenbloom, who was a fantastic mentor to me both professionally and personally, and really helped me grow and survive as a researcher and as a person these past few years, in addition to Christina Fuentes and Prajit Limsirichai, whose empathy, great humor, and taste in comfort food were a constant bright spot when things stopped working in the lab.

I’d like to thank my friends and family. In particular, my parents, without whose support and understanding I’d never have made it this far. I owe them my thanks for always being there for me, especially when things were uncertain or tough, and for going out of your way to support and help me when I needed it (which was often).

And last, I’d like to thank my partner of four years, Alyssa Wong. Your humor, energy, love, and support over the years got me through the darkest days and made even the happiest moments even sweeter. Thank you for always being here for me, even when things are hard, for never giving up on me, for never letting me down.

Chapter 1: Neural Stem Cells Development and Differentiation

For the better part of a century, it was a widely held assumption within the field of neuroscience that no new neurons were added to the adult mammalian brain after adolescence.[1] As the brain showed no gross changes in morphology, and initial characterizations of neurons displayed no signs of mitotic potential or activity, foundational researchers in neuroanatomy had no reason to believe that adult neurogenesis might be possible. However, the first seeds of change were planted by a then little-read study in the 1960's conducted by Joseph Altman and Gopal Das[2]. By conducting injections of radioactively labeled thymidine into young rats, they observed significant labeling of granule cells in the hippocampal dentate gyrus, suggesting ongoing cellular division and differentiation into neurons into adolescence. By the end of the 1990's, after a tumultuous adolescence, the study of adult neurogenesis had found evidence of continuing neuronal differentiation in a variety of animals, including rat,[3] rabbit,[4] monkey,[5] and, most sensationally, humans.[6] Since then our understanding of neural stem cell (NSC) behavior and the properties of their stem cell niche has grown dramatically.

We now know that hippocampal NSCs play an ongoing role in maintaining learning and memory formation,[7,8] and know that their dysfunction is often correlated with many neurodegenerative diseases, such as Alzheimers.[9] We know that the stem cell niche is an exquisite balance of forces, with many convergent signaling pathways and molecules dictating the pattern of NSC development and differentiation. Signaling factors that regulate proliferation such as Notch[10], Sonic hedgehog[11], VEGF[7], or differentiation such as Wnt[12] and EphrinB2[13] have all been identified and studied as elements of the niche that are capable of controlling NSC behavior. Recently, studies have begun to probe some of the underlying physical properties of the niche as well, such as substrate elastic modulus[14,15], adding new dimensionality to our understanding of the complex, multifactorial stem cell niche.

However, recent studies have begun to illuminate the enormity of the task of deciphering stem cell behavior and engineering control of differentiation. Since the acceptance of adult neurogenesis in select regions of the brain, modern researchers have rapidly identified the signaling pathways that regulate differentiation and proliferation, and how these pathways overlap with various stages of cellular development and fate commitment (Figure 1). However, rather than being an additive combination of forces upon NSCs, these various pathways engage in significant crosstalk and respective activation or repression. For example, Wnt and Notch can oppose one another[16], Wnt can upregulate BDNF[17], Shh, Wnt, and BDNF can interact with one another in pathological phenotypes[18], and many pro-proliferative pathways such as PI3K-Akt signal through or from Hippo[19]. Discovering, deciphering, and engineering these complex, multi-component and highly interwoven pathways is crucial for progress in stem cell biology and engineering.

In this work, we investigate the influence of mechanical, extracellular cues on NSC differentiation by measuring and recapitulating elements of the niche, and dissecting the downstream activated molecular pathways. We investigate the variations in mechanical environment in the endogenous niche, and then recapitulate similar variations in engineered, *in vitro* conditions and examined how mechanotransducers such as YAP/TAZ carry the signals of the ECM to neurogenic pathways. We conclude this work by examining the effect of matrix dimensionality and composition, rather than simple substrate modulus, and find that brain-

mimetic matrices are able to robustly guide neurogenesis in NSCs. Together these results help elucidate new key elements of NSC biology and improve our ability to control and engineer the NSC niche.

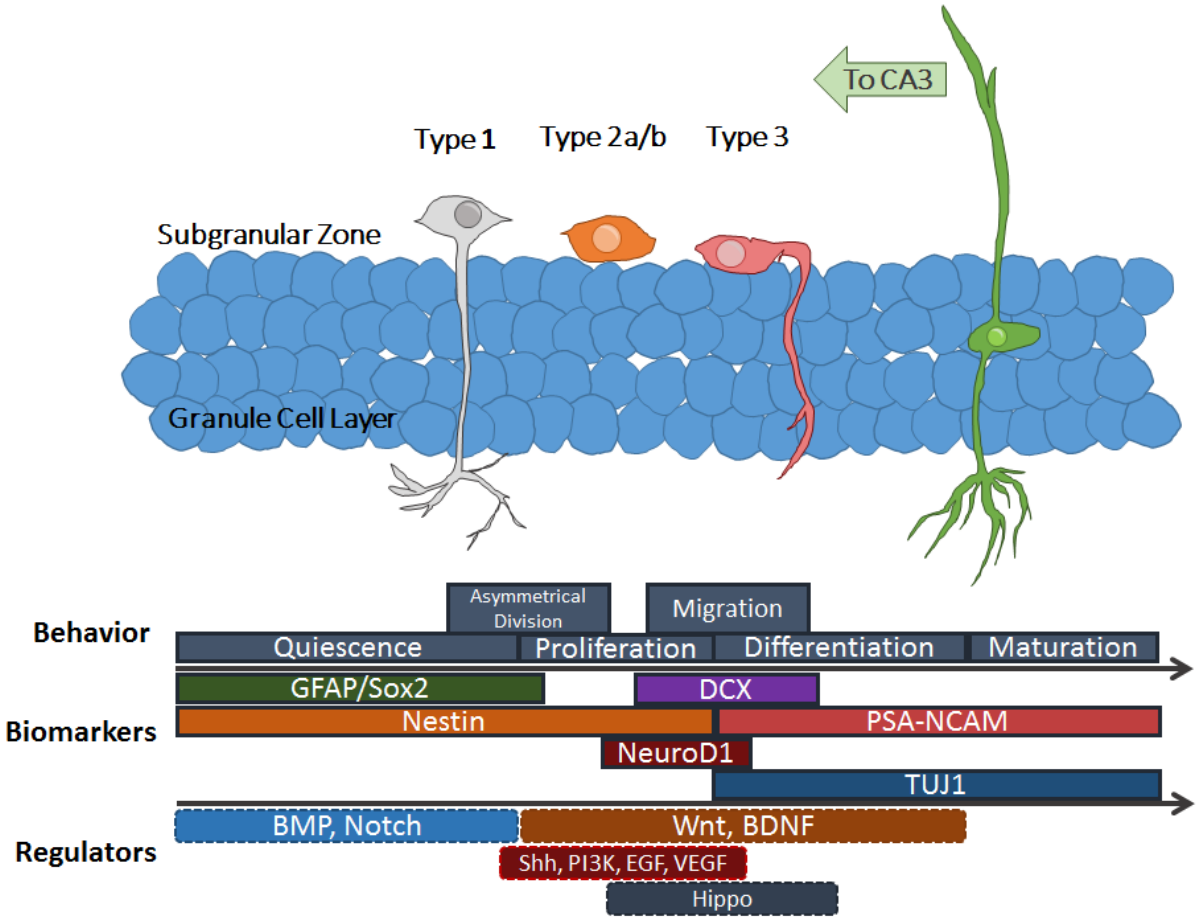

Figure 1: Subgranular zone NSC life cycle and differentiation. Type 1 radial glia-like stem cells represent the quiescent stem cell pool in the hippocampal niche. When induced to exit quiescence, they begin rapid, asymmetrical cell division to yield type 2a transit-amplifying neural progenitors. These begin as Nestin+, gain DCX+ with maturation (type 2b) and lose Nestin+ and they gain PSA-NCAM+ (type 3 neuroblasts). These cells then exit into a committed, TUJ1+ immature neuronal phenotype. As the cells continue to mature, they migrate further into the granule cell layer and rapidly extend axons along the mossy fiber pathway towards the CA3 pyramidal cell layer, while their apical dendrites grow through the granule cell layer and project into the molecular layer.

Works Cited

1. Gross, C. G. Neurogenesis in the adult brain: death of a dogma. *Nat. Rev. Neurosci.* **1,** 67–73 (2000).

2. Altman, J. & Das, G. D. Autoradiographic and histological evidence of postnatal hippocampal neurogenesis in rats. *J. Comp. Neurol.* **124,** 319–335 (1965).

3. Kuhn, H. G., Dickinson-Anson, H. & Gage, F. H. Neurogenesis in the dentate gyrus of the adult rat: age-related decrease of neuronal progenitor proliferation. *J. Neurosci.* **16,** 2027–33 (1996).

4. Guéneau, G., Privat, A., Drouet, J. & Court, L. Subgranular zone of the dentate gyrus of young rabbits as a secondary matrix. A high-resolution autoradiographic study. *Dev. Neurosci.* **5,** 345–58 (1982).

5. Gould, E., Tanapat, P., McEwen, B. S., Flügge, G. & Fuchs, E. Proliferation of granule cell precursors in the dentate gyrus of adult monkeys is diminished by stress. *Proc. Natl. Acad. Sci. U. S. A.* **95,** 3168–71 (1998).

6. Eriksson, P. S. *et al.* Neurogenesis in the adult human hippocampus. *Nat. Med.* **4,** 1313–1317 (1998).

7. Cao, L. *et al.* VEGF links hippocampal activity with neurogenesis, learning and memory. *Nat. Genet.* **36,** 827–835 (2004).

8. Deng, W., Aimone, J. B. & Gage, F. H. New neurons and new memories: how does adult hippocampal neurogenesis affect learning and memory? *Nat. Rev. Neurosci.* **11,** 339–350 (2010).

9. Mu, Y. & Gage, F. H. Adult hippocampal neurogenesis and its role in Alzheimer's disease. *Mol. Neurodegener.* **6,** 85 (2011).

10. Breunig, J. J., Silbereis, J., Vaccarino, F. M., Sestan, N. & Rakic, P. Notch regulates cell fate and dendrite morphology of newborn neurons in the postnatal dentate gyrus. *Proc. Natl. Acad. Sci.* **104,** 20558–20563 (2007).

11. Lai, K., Kaspar, B. K., Gage, F. H. & Schaffer, D. V. Sonic hedgehog regulates adult neural progenitor proliferation in vitro and in vivo. *Nat. Neurosci.* **6,** 21–27 (2002).

12. Lie, D.-C. *et al.* Wnt signalling regulates adult hippocampal neurogenesis. *Nature* **437,** 1370–1375 (2005).

13. Ashton, R. S. *et al.* Astrocytes regulate adult hippocampal neurogenesis through ephrin-B signaling. *Nat. Neurosci.* **15,** 1399–1406 (2012).

14. Saha, K. *et al.* Substrate modulus directs neural stem cell behavior. *Biophys. J.* **95,** 4426–38 (2008).

15. Keung, A. J., de Juan-Pardo, E. M., Schaffer, D. V. & Kumar, S. Rho GTPases Mediate the Mechanosensitive Lineage Commitment of Neural Stem Cells. *Stem Cells* **29,** 1886–1897 (2011).

16. VanHook, A. M. Dishevelled Mediates Wnt-Notch Crosstalk. *Sci. Signal.* **5,** ec298-ec298 (2012).

17. Yi, H., Hu, J., Qian, J. & Hackam, A. S. Expression of brain-derived neurotrophic factor is regulated by the Wnt signaling pathway. *Neuroreport* **23,** 189–94 (2012).

18. Tayyab, M. *et al.* Sonic hedgehog, Wnt, and brain-derived neurotrophic factor cell signaling pathway crosstalk: potential therapy for depression. *J. Neurosci. Res.* **96,** 53–62 (2018).

19. Tumaneng, K. *et al.* YAP mediates crosstalk between the Hippo and PI(3)K–TOR pathways by suppressing PTEN via miR-29. *Nat. Cell Biol.* **14,** 1322–1329 (2012).

Chapter 2: Stiffness Variations in the Dentate Gyrus

Reprinted with permission from the Royal Society, from the article "Microelastic mapping of the rat dentate gyrus", by Tomás Luque, Michael S. Kang, David V. Schaffer, and Sanjay Kumar in Journal of the Royal Society Open Science, 3(4): 2016.

Abstract

The lineage commitment of many cultured stem cells, including adult neural stem cells (NSCs), is strongly sensitive to the stiffness of the underlying extracellular matrix. However, it remains unclear how well the stiffness ranges explored in culture align with the microscale stiffness values stem cells actually encounter within their endogenous tissue niches. To address this question in the context of hippocampal NSCs, we used atomic force microscopy to spatially map the microscale elastic modulus (E) of specific anatomical substructures within living slices of rat dentate gyrus in which NSCs reside during lineage commitment in vivo. We measured depth-dependent apparent E-values at locations across the hilus (H), subgranular zone (SGZ) and granule cell layer (GCL) and found a two- to threefold increase in stiffness at 500 nm indentation from the H (49 ± 7 Pa) and SGZ (58 ± 8 Pa) to the GCL (115 ± 18 Pa), a fold change in stiffness we have previously found functionally relevant in culture. Additionally, E exhibits nonlinearity with depth, increasing significantly for indentations larger than 1 μm and most pronounced in the GCL. The methodological advances implemented for these measurements allow the quantification of the elastic properties of hippocampal NSC niche at unprecedented spatial resolution.

Introduction

Neural stem cells (NSCs), which reside in the hippocampus and the subventricular zone of the adult mammalian brain, continually generate neurons throughout adult life [1,2]. Hippocampal NSCs reside in the subgranular cell layer (SGZ) of the dentate gyrus (DG), undergo self-renewal and neuronal differentiation throughout adult life and play key roles in learning and memory. Differentiation is a coordinated process involving migration over several cell diameters into the granule cell layer (GCL), extension of axons through the hilus (H) and into CA3, and development of dendrites through the GCL and into the molecular layer [1,3,4].

Importantly, this process is not static but dynamically responds to numerous cellular and molecular inputs. For instance, key biochemical signalling factors within the SGZ microenvironment have been found to regulate both neural stem and progenitor cell proliferation—such as sonic hedgehog [5], fibroblast growth factor-2, heparin-binding EGF-like growth factor [6] and vascular endothelial growth factor [7]—and neuronal differentiation—such as Wnt3a [8,9] and ephrin-B2 [10]. Additionally, not only the biochemical but also the biophysical microenvironment may regulate stem cell function. For example, mechanical signalling through cell–extracellular matrix (ECM) interactions has been shown to play a role in regulating NSC differentiation. In particular, the elastic modulus (E) of the ECM substrate has been shown to regulate NSC lineage in vitro [11,12], with soft ECMs promoting NSC neurogenesis and stiff ECMs suppressing it [12,13]. Despite the clear instructive effects of elastic modulus on stem cell behaviour in vitro, and the in vivo regulation of stem cell behaviour

by signals that are modulated in vitro by stiffness differences [13], the degree to which E may vary in the in vivo niche is unknown.

Atomic force microscopy (AFM) indentation has facilitated direct measurement of E with higher (up to sub-micrometre) spatial resolution compared with other methods such as optical coherence tomography [14] and stress-relaxation micro-indentation [15], and has been used notably by Morrison and co-workers to map and report stiffness across the rat hippocampus bulk from the CA1 to CA3 pyramidal cell layers and across the DG [16]. Such measurements have informed the design of in vitro assay platforms capable of recapitulating in vivo behaviour. Synthetic polyacrylamide matrix culture systems have shown stiffness-dependent instruction of NSC differentiation [12,13], neurogenic instruction of pluripotent stem cell differentiation [17] and full neuronal maturation and subtype differentiation with physiological stiffness values [18]. That said, these seminal AFM indentation measurements focused on large size scale variations in stiffness across the entire hippocampus, rather than high-resolution investigation of the specific regions in which hippocampal NSCs reside. While technically challenging, obtaining higher resolution mechanical maps of portions the hippocampal NSC niche relevant to neurogenesis could provide valuable insight into potential mechanical influences on NSCs during proliferation and differentiation in vivo. To address this unmet need, we conducted AFM measurements of the elastic modulus of the DG between the GCL and H, a region that directly encompasses the stem cell niche.

Methods and Materials

Murine hippocampus preparation

Coronal hippocampal sections were prepared as described previously [26]. Briefly, juvenile (p18–p22) Sprague–Dawley rats were anaesthetized with isoflurane and sacrificed by decapitation. The brain was extracted and kept in a low-sodium, bicarbonate-buffered cutting solution at ambient temperature with constant bubbling with 95% O2 and 5% CO2, and 400 μm coronal sections were cut with a Leica VT1000S vibratome at 0°C. The sections were stored in Ringer's solution at ambient temperature and bubbling with 95% O2 and 5% CO2 and were quickly transported to the AFM stage. Sections were gently weighed down for measurement on a Petri dish with parallel nylon fibres (approx. 2 mm spacing) attached to a metal ring, and measured within 30–60 min after sacrifice. Cutting solution composition was 75 mM sucrose, 85 mM NaCl, 25 mM NaHCO3, 25 mM d-(+)-glucose, 2.5 mM KCl, 1.25 mM NaH2PO4–H2O, 0.5 mM ascorbic acid, 4 mM MgCl2, 0.5 mM CaCl2, 320 mOsm l−1, pH 7.2.

Atomic force microscopy measurements

Indentation measurements were obtained with a NanoScope Catalyst (Bruker Corporation, Billerica, MA, USA) atomic force microscope mounted on an inverted optical microscope (Eclipse Ti-E, Nikon Corporation, Chiyoda, Tokyo, Japan). A 25 μm diameter polystyrene bead (Polysciences, Inc., Warrington, PA, USA) was epoxied to the end of a soft ($k = 0.01$ N m−1) tipless cantilever (MLCT-O10, Bruker). The combination of a soft cantilever and a large bead (compared with the indentation) allowed us to measure the small deflections that such soft samples caused on the cantilever. Fabrication was validated with scanning electron microscopy, and cantilever spring constants (k) were measured via thermal oscillation [27] using an Asylum MFP-3D Infinity AFM (Asylum Research, Santa Barbara, CA, USA).

For each sample, five linear profiles transverse to the DG layers were acquired (indicated by lines in figure 1). Seven measurements were taken across each profile, with the centre point directly on the SGZ and a lateral spacing of 50 μm. Each measurement was the average of five force curves, obtained with ramp amplitude of 10 μm and frequency of 0.5 Hz, resulting in tip velocity of 10 μm s−1.

Data processing

The force *F* exerted on the cantilever was calculated as a Hookean linear spring:

$$F = k\,(d - d_0) \tag{1}$$

And indentation depth δ was defined as:

$$\delta = (z - z_c) - (d - d_0) \tag{2}$$

With d as cantilever deflection, d_0 as deflection offset, z as cantilever vertical position, z_c as cantilever vertical position at the contact point. This data was fit to the Hertz contact model for a sphere indenting an infinite sphere using a non-linear least-squares method[19]:

$$F = \frac{4\hat{E}}{3(1-v^2)} R^{1/2}\delta^{3/2} \tag{3}$$

with R defined as bead radius (12.5 μm) and v as Poisson's ratio. We assumed a Poisson's ratio of 0.5, which agrees closely with simulation [28] and past measurements [29]. We fitted a two-part equation (a line for the non-contact zone and the Hertz elastic model for the contact zone) to the entire dataset using a nonlinear least-squares method (Matlab, The MathWorks, Natick, MA, USA) to obtain an estimation of the contact point (zc, d0). We iterated the fit using a defined maximum indentation (δmax) to refine our estimation of the contact point and E. Additional fittings did not appreciably improve the error. We report a pointwise apparent Young's modulus ($\hat{E}(\delta)$), reported at three chosen indentations (500 nm, 1 μm and 1.5 μm). Statistical analysis was performed with a two-way repeated measures analysis of variance (Sigma Plot, Systat Software), with factors region and indentation.

Results

Preparation of hippocampal slices for atomic force microscopy stiffness mapping

To maximally preserve physiological biomechanical properties of brain tissue, we designed a protocol for much more rapid (less than 1 h after sacrifice), fixative-free AFM measurements of hippocampal slices. Briefly, we extracted brains from freshly sacrificed rats and immersed them in 0°C cutting solution. We used a vibratome to generate 400 μm thick coronal sections, and quickly transported sections to the AFM stage. To save time that would normally be needed to allow adhesive bonding of the sample to the substrate, we secured the slices by placing them under a nylon mesh secured by a metal ring. A compliant nylon mesh with wide spacing (2 mm) was used to minimize tissue deformation and strain near the point of measurement. AFM measurements were performed between 30 and 60 min after sacrifice (figure 1). Importantly, our protocol uses no chemical fixatives and minimal embedding, and the AFM tip is allowed to directly contact the tissue surface. A thick sample (400 μm) and small indentation depths (less than 2 μm) were used to prevent the underlying polystyrene dish from contributing to measurements.

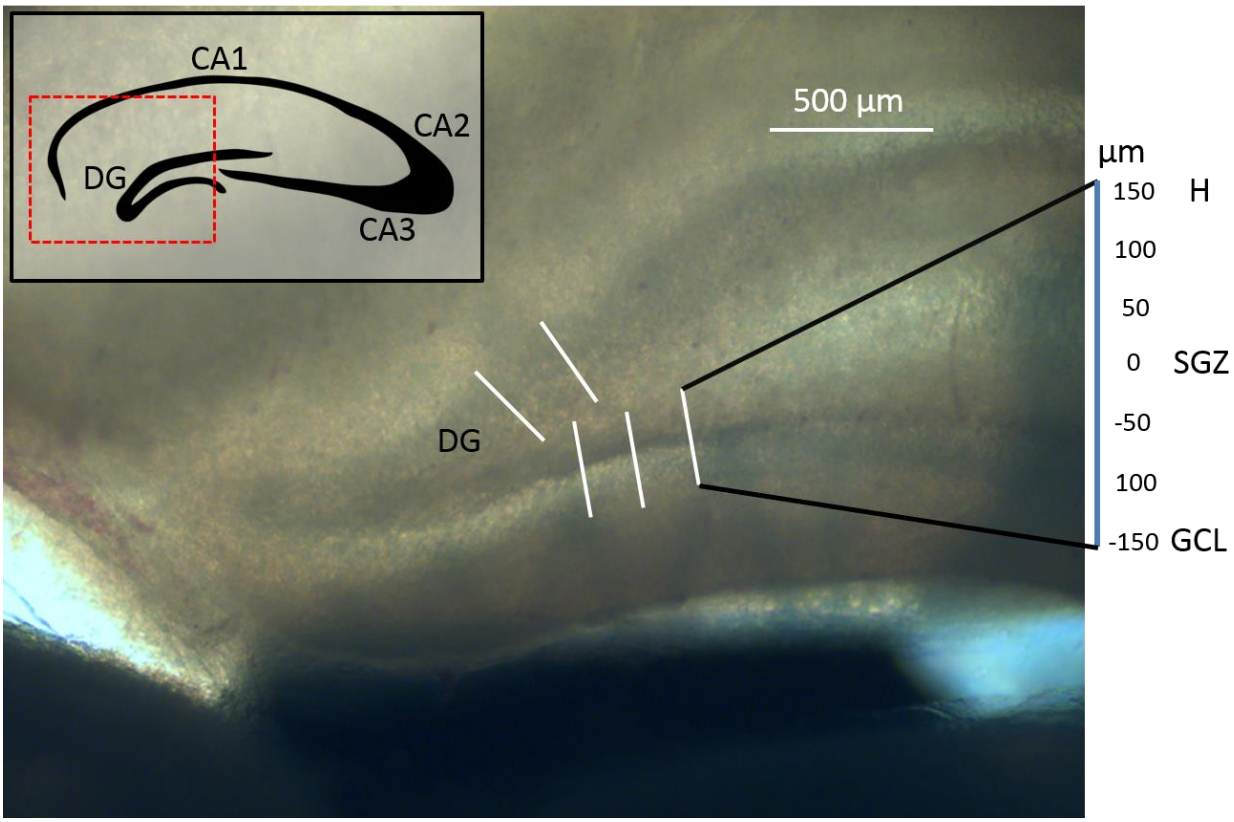

Figure 2: Transmitted light image of a representative coronal hippocampal section. Measurements were taken in the DG, at 7 points along a 300µm linear profile from the GCL to the H. Five profiles for each slice were taken, and representative measurement locations are indicated.

Stiffness is variable across the stem cell niche

Five linear profiles of force curves were acquired in six samples (figure 1), up to an estimated indentation of 2 µm. The contact point was algorithmically estimated, and force curves were fitted to the Hertz contact model for a sphere indenting up to a maximum indentation (δmax) of 500 nm. Owing to the large polystyrene bead (25 µm) used as a tip, measurements incorporate both cell and matrix mechanical properties. Two iterations of a nonlinear fit were used to obtain E (figure 2a). The mean at 500 nm indentation was 49 ± 7 Pa (mean ± s.e., $N = 6$) for the H, 58 ± 8 Pa in the SGZ and 115 ± 18 Pa in the GCL (figure 2a). These values are comparable with previous reports of E as approximately 100 Pa in the DG for a 500 nm indentation [16]. However, we discovered that the GCL stiffness was significantly ($p < 0.01$, two- to threefold increase) higher than the SGZ and the H, whereas comparisons between the SGZ and H showed no significant difference ($p > 0.05$). The measurements thus indicate a gradient of increasing stiffness between the SGZ and the GCL (figure 2a), which has not been previously observed.

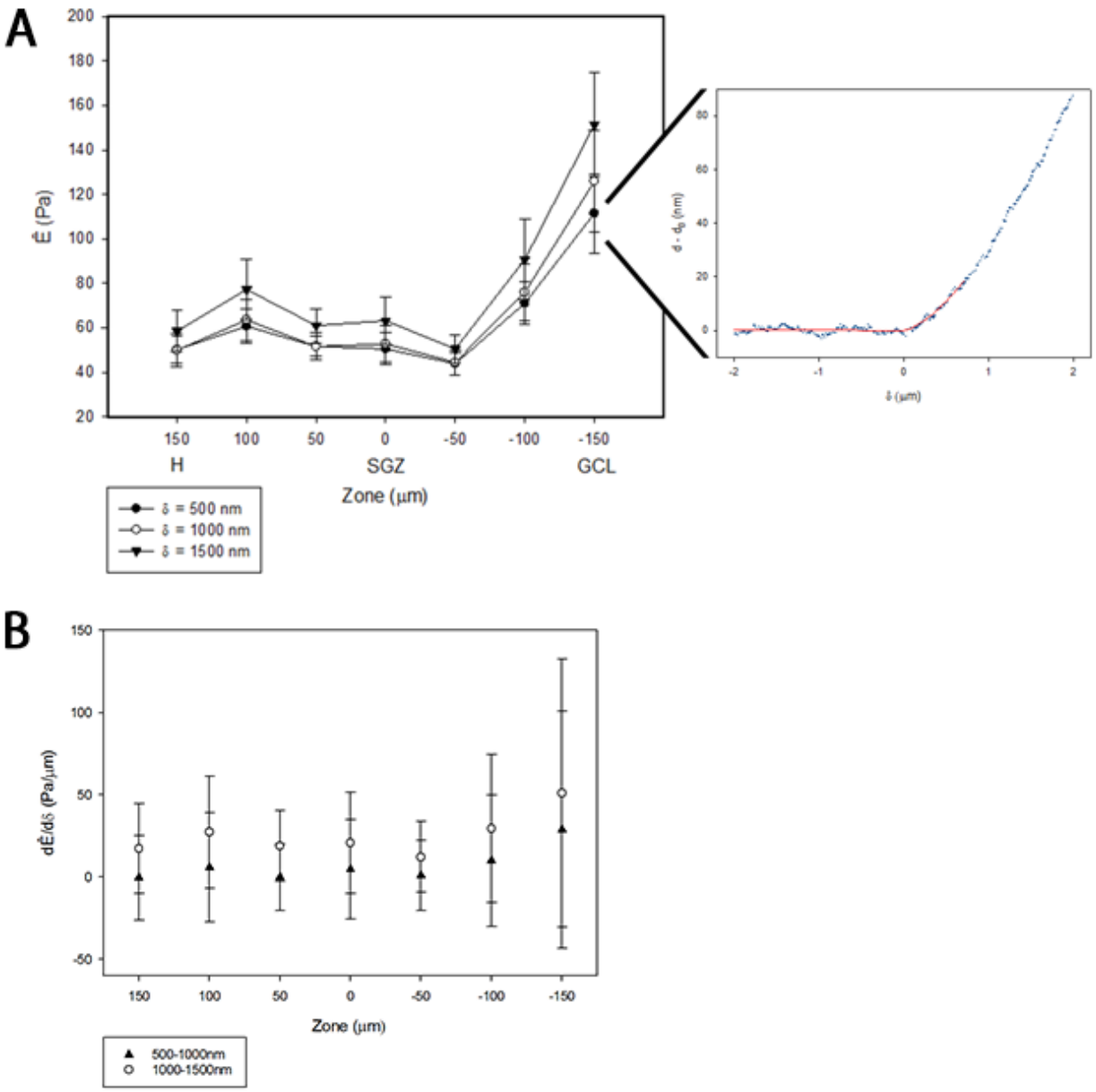

Figure 3: **A**. Average E from 6 brain samples with representative force curve. In the inset representative force curve, points depict experimental data for z, cantilever vertical position, and d, cantilever deflection, and the trend line is a two-part fitted model: a straight line for the non-contact zone and a 3/2 power of δ for the contact region. In the graph, each point is the average of 5 force curves, and shown for 3 different indentation depths. The tissue is slightly nonlinear with indentation depth. Standard error is indicated. Stiffness in H and SGZ are significantly different from GCL ($p < 0.05$). SGZ & GCL both showed significant differences between δ = 1000 nm and δ = 1500 nm. SGZ showed significant difference between δ = 500 nm and δ = 1000 nm. **B**. Graph of derivative of Ê with respect to indentation depth, indicating the depth dependence of strain stiffening.

Dentate gyrus stiffness exhibits slight nonlinearity for indentations greater than 1 µm

Tissue behaviour (linear or nonlinear) at supraphysiological strains is a critical component for understanding response to injury, and the hippocampus in particular is uniquely sensitive to mechanical strain [19]. We therefore computed a pointwise, depth-dependent apparent Young's modulus ($\hat{E}$) at indentations of 0.5, 1 and 1.5 µm. At a greater indentation depth, the sample exhibited higher stiffness values than at lower depths for particular locations. Specifically, $\hat{E}$ ($\delta = 500$ nm) was 50 ± 6 Pa (H), 51 ± 7 Pa (SGZ) and 111 ± 18 Pa (GCL), but with $\delta = 1500$ nm these values increased to 59 ± 9 Pa, 63 ± 11 Pa and 151 ± 24 Pa, respectively (figure 2a,b). Both the SGZ and the GCL exhibited significant differences ($p < 0.05$) in $\hat{E}$ between 1 and 1.5 µm indentations, but only the SGZ showed a difference between 0.5 and 1 µm. While tissue nonlinearity has been previously reported for the DG bulk as between 90 and 130 Pa [16], differences in nonlinearity have not been observed within the sub-anatomical regions of the hippocampus and NSC niche.

Discussion

In this study, we spatially mapped the elastic modulus of the hippocampal NSC niche using AFM. Our work both represents a key methodological advance and reveals new insight into the micromechanical properties of the endogenous NSC niche, thereby providing crucial design input for systems to recapitulate NSC neurogenesis in vitro. Methodologically, our approach is expected to preserve key mechanical properties of brain tissue by employing no chemical fixation and only minimal embedding, as well as by reducing preparation time by physically anchoring rather than adhesively bonding the tissue to the substrate. Additionally, our approach incorporates automated identification AFM tip contact points, similar to methods previously reported [20,21], which have typically been identified by visual examination. This invites error and observer bias that may significantly affect the resulting curve fit and extraction of E and $\hat{E}$. While important advances have been made to automate this process through the use of algorithmic models, these approaches rely on empirically determined criteria to define the contact point. Moreover, these models are suited for samples at least an order of magnitude stiffer than brain tissue and have difficulty identifying contact points for very soft gels <3 kPa [22]. To remedy this concern, we used an algorithmic, iterative fitting procedure that defines a contact point based on contact theory, which allowed us to identify the contact point more reproducibly and systematically.

These advances in sample preparation, together with the high spatial resolution of AFM, allowed us to spatially map DG substructures and identify differences in stiffness across regions of the DG, which has not been yet evaluated with high resolution. The SGZ, where the progenitor pool is maintained, and the H, through which new axons grow and project to the CA3, both show stiffness near 50 Pa. The GCL, through which newly differentiated neurons migrate and extend dendrites, shows twofold higher stiffness. The difference in stiffness in the GCL may be due to the densely packed mature granule cells, whereas the lower stiffness in the SGZ and H may be due to differences in cell body density, or even possibly different mechanical properties of immature progenitors. These measurements show that among these anatomical features, there are stiffness gradients that are in a position to influence cell differentiation and axonal and dendritic growth. Additionally, we have identified substructure specific nonlinear stiffening for indentations higher than a micrometre, which indicates possible heterogeneities between tissue substructures, such as differences in cell body and nuclei density between regions. Previous work

has identified the hippocampus bulk as possessing strain-stiffening properties, we have shown and characterized precise values for the DG, and notably see this behaviour in the SGZ and GCL but not in the H. While these results are compatible with the observation that many biopolymers can exhibit strain-stiffening behaviour, the reason for this and its physiological implications are unknown and may be the subject of future work [23]. Finally, synthetic systems used to study NSC differentiation have to date been uniform in stiffness, and future work with new culture platforms may explore whether microscale stiffness gradients could serve an informative role in neural stem cell development.

Our measurements also validate the physiological relevance of engineered ECM substrates to drive NSC neurogenesis in culture. We show that the stiffness of living DG tissue lies within a range of 50–150 Pa, which is consistent with past AFM measurements of bulk hippocampal tissue [16] and closely matches stiffness regimes previously identified (200 Pa in two-dimensional culture [12,13] and 180 Pa in three-dimensional culture [24]) to be pro-neurogenic in vitro for NSCs, mesenchymal stem cells [11] and human pluripotent stem cells [17]. However, it is important to note some caveats that accompany our measurements. While reducing sample preparation time and removing fixation steps are expected to preserve physiological properties of brain, indentation measurements are still taken on a cut surface of a brain slice. This can cause significant cell death and relaxation in the brain matrix in the plane of indentation. Additionally, in order to better preserve tissue properties, measurements were obtained in buffer at refrigerant temperature (4°C) rather than body temperature, which may produce some artefactual stiffening due to tissue contraction. Last, our study examines only juvenile rats at P18–22, while neurogenesis is an ongoing process, especially in adults. Indeed, the stiffness of bulk hippocampus has been shown to vary by more than 100% between P10 and adulthood [25]. Nevertheless, our measurements therefore offer key, novel validation to these materials strategies by demonstrating that these pro-neurogenic stiffness values match well with the stiffness of microscale regions associated with NSC proliferation (SGZ) and differentiation (GCL) in the hippocampus.

It is anticipated that further methodological refinements may enable even higher-resolution mapping of these niches, which in turn may yield more sophisticated input into the design of neurogenic culture scaffolds. Additionally, it would be useful to revisit these measurements with specific hippocampal disease models to investigate potential biomechanical changes in the NSC niche that may influence neurogenesis in currently unappreciated ways. Finally, by coupling these AFM measurements with live cell markers that track specific stages of neural lineage commitment maturation, it may be possible to correlate changes in microscale tissue mechanics within the DG with the dynamics of neurogenesis. With the emergence of increasingly sophisticated materials strategies that enable patterning of ECM stiffness in time and space, such measurements help the field discover and recapitulate subtleties of the NSC niche.

Acknowledgements

We gratefully acknowledge the laboratories of Dr. Daniel Feldman and Dr. Daniela Kaufer at UC Berkeley, especially Dr. Justin Elstrott, for contributing some of the rat brains used in this study and for technical guidance on slice preparation. This work was supported by a grant from the NIH (1R01NS074831 to D.V.S. and S.K.) and from the Spanish Ministry of Education (FPU grant with BOE October 28th 2008 to T.L). We thank The Royal Society Publishing for

permission to republish work originally published in: "Microelastic mapping of the rat dentate gyrus," Royal Society Open Science, 2016 Apr; 3(4): 150702. by Tomás Luque, Michael S. Kang, David V. Schaffer, and Sanjay Kumar.

References

1. Deng, W., Aimone, J. B. & Gage, F. H. New neurons and new memories: how does adult hippocampal neurogenesis affect learning and memory? *Nat Rev Neurosci* **11,** 339–350 (2010).
2. Gage, F. H. Mammalian Neural Stem Cells. *Science (80).* **287,** 1433–1438 (2000).
3. Kempermann, G. & Gage, F. H. Genetic influence on phenotypic differentiation in adult hippocampal neurogenesis. *Dev. Brain Res.* **134,** 1–12 (2002).
4. Santarelli, L. *et al.* Requirement of Hippocampal Neurogenesis for the Behavioral Effects of Antidepressants. *Science* **301,** 805–809 (2003).
5. Lai, K., Kaspar, B.K., Gage, F.H. & Schaffer, D.V. Sonic hedgehog regulates adult neural progenitor proliferation in vitro and in vivo. *Nat Neurosci*. **6,** 21–27 (2003).
6. Jin, K. *et al.* Neurogenesis and aging: FGF-2 and HB-EGF restore neurogenesis in hippocampus and subventricular zone of aged mice. *Aging Cell* **2**, 175–183 (2003).
7. Cao, L. *et al*. VEGF links hippocampal activity with neurogenesis, learning and memory. *Nat. Genet*. **36**, 827–835 (2004).
8. Lie, D.-C. *et al.* Wnt signalling regulates adult hippocampal neurogenesis. *Nature* **437,** 1370–1375 (2005).
9. Kuwabara, T. *et al.* Wnt-mediated activation of NeuroD1 and retro-elements during adult neurogenesis. *Nat Neurosci* **12,** 1097–1105 (2009).
10. Ashton, R. S. *et al.* Astrocytes regulate adult hippocampal neurogenesis through ephrin-B signaling. *Nat Neurosci* **15,** 1399–1406 (2012).
11. Engler, A. J., Sen, S., Sweeney, H. L. & Discher, D. E. Matrix Elasticity Directs Stem Cell Lineage Specification. *Cell* **126,** 677–689 (2006).
12. Saha, K. *et al.* Substrate Modulus Directs Neural Stem Cell Behavior. *Biophys. J.* **95,** 4426–4438 (2008).
13. Keung, A. J., de Juan-Pardo, E. M. Schaffer, D. V., & Kumar, S. Rho GTPases mediate the mechanosensitive lineage commitment of neural stem cells. *Stem Cells* **29,** 1886–1897 (2011).
14. Lee, S. J. *et al.* Measurement of viscoelastic properties in multiple anatomical regions of acute rat brain tissue slices. *J. Mech. Behav. Biomed. Mater.* **29,** 213–224 (2014).
15. Elkin, B. S., Ilankovan, A. I. & Morrison, B. A Detailed Viscoelastic Characterization of the P17 and Adult Rat Brain. *J. Neurotrauma* **28,** 2235–2244 (2011).
16. Elkin, B. S., Azeloglu, E. U., Costa, K. D. & Morrison III, B. Mechanical Heterogeneity of 7the Rat Hippocampus Measured by Atomic Force Microscope Indentation. *J. Neurotrauma* **24,** 812–822 (2007).

17. Keung, A. J., Asuri, P., Kumar, S., & Schaffer, D. V. Soft microenvironments promote the early neurogenic differentiation but not self-renewal of human pluripotent stem cells. *Integr. Biol.* **4,** 1049–1058 (2012).
18. Keung, A. J., Dong, M., Schaffer, D. V., & Kumar, S. Pan-neuronal maturation but not neuronal subtype differentiation of adult neural stem cells is mechanosensitive. *Sci. Rep.* **3,** 1817 (2013).
19. Lin D.C., Dimitriadis E.K., Horkay F. Robust strategies for automated AFM force curve analysis--I. Non-adhesive indentation of soft, inhomogeneous materials. *J Biomech Eng*. 430-40. (2007)
20. Costa, K.D. Imaging and Probing Cell Mechanical Properties With the Atomic Force Microscope. *Methods Mol Biol*. 331–361 (2006)
21. Atkins, C.M. Decoding hippocampal signaling deficits after traumatic brain injury. *Transl Stroke Res.* 546-55 (2011).
22. Thomas, G., Burnham, N. a, Camesano, T. A. & Wen, Q. Measuring the mechanical properties of living cells using atomic force microscopy. *J. Vis. Exp.* 1–8 (2013).
23. Erk, K. a., Henderson, K. J. & Shull, K. R. Strain stiffening in synthetic and biopolymer networks. *Biomacromolecules* **11**, 1358–1363 (2010).
24. Banerjee, A., et al. The Influence of Hydrogel Modulus on the Proliferation and Differentiation of Encapsulated Neural Stem Cells. *Biomaterials,* **30,** 4695–4699 (2009).
25. Elkin, B. S., Ilankovan A & Morrison III, B. Age-dependent regional mechanical properties of the rat hippocampus and cortex. *J Biomech Eng*. 132 (2010).
26. House, D. R., Elstrott, J., Koh, E., Chung, J. & Feldman, D. E. Parallel regulation of feed forward inhibition and excitation during whisker map plasticity. *Neuron* **72,** 819–831 (2011).
27. Hutter, J. L. & Bechhoefer, J. Calibration of atomic-force microscope tips. *Rev. Sci. Instrum.* **64,** 1868–1873 (1993).
28. Soza, G. *et al.* Determination of the elasticity parameters of brain tissue with combined simulation and registration. *Int. J. Med. Robotics Comput. Assist. Surg.* **1,** 87–95 (2005).
29. Gefen, A., Gefen, N., Zhu, Q., Raghupathi, R. & Margulies, S. S. Age-Dependent Changes in Material Properties of the Brain and Braincase of the Rat. *J. Neurotrauma* **20,** 1163–1177 (2003).

Chapter 3: YAP-mediated Temporal Dynamics of Mechanosensitive Neural Stem Cell Differentiation

Reprinted with permission from John Wiley & Sons, from the article "Dynamics of Mechanosensitive Neural Stem Cell Differentiation", by Sebastian Rammensee, Michael S Kang, Katerina Georgiou, Sanjay Kumar, and David V. Schaffer in Stem Cells, 35(2), 497-506: 2016.

Abstract

Stem cell differentiation can be highly sensitive to mechanical inputs from the extracellular matrix (ECM). Identifying temporal windows during which lineage commitment responds to ECM stiffness, and the signals that mediate these decisions, would advance both mechanistic insights and translational efforts. To address these questions, we investigate adult neural stem cell (NSC) fate commitment using an oligonucleotide-crosslinked ECM platform that for the first time offers dynamic and reversible control of stiffness. "Stiffness pulse" studies in which the ECM was transiently or permanently softened or stiffened at specified initiation times and durations pinpoint a 24-hour window in which ECM stiffness maximally impacts neurogenic commitment. Overexpression of the transcriptional coactivator Yes-associated protein (YAP) within this window suppressed neurogenesis, and silencing YAP enhanced it. Moreover, ablating YAP-b-catenin interaction rescued neurogenesis. This work reveals that ECM stiffness dictates NSC lineage commitment by signaling via a YAP and b-catenin interaction during a defined temporal window.

Introduction

Stem cell self-renewal and differentiation are tightly controlled by the cellular microenvironment or "niche," which presents a spectrum of soluble and immobilized biochemical signals and biophysical cues [1]. Among this latter class of inputs, mechanical cues encoded in the extracellular matrix (ECM) are increasingly recognized as important regulators of lineage commitment in many types of stem cells [2]. For example, we previously showed that ECM stiffness variations in the range of 1–10 kPa strongly bias the neuronal versus astrocytic differentiation of adult neural stem cells (NSCs) [3, 4]. These findings are important both in designing material scaffolds for biomedical applications and for our understanding of NSC biology in vivo, where hippocampal NSCs are exposed to anatomic stiffness gradients as they migrate into the dentate gyrus and undergo neuronal differentiation and maturation [1, 5].

Despite several recent advances, much remains unknown about the molecular mechanisms that connect mechanical inputs to stem cell differentiation. As a prominent example, cells typically sense ECM stiffness cues over seconds to minutes [6], yet it is unclear over what time scales stem cells integrate these cues and execute lineage commitment decisions that only fully declare themselves with changes in marker expression and cellular function days to weeks later. For instance, we recently showed that NSCs adapt their intrinsic mechanical properties to those of the ECM within 12 hours of seeding and that transient pharmacological inhibition of mechanosensing pathways can abrogate downstream marker expression and differentiation that occurs 4-6 days after adhesion [4]. Similarly, traction forces generated by human mesenchymal stem cells (MSCs) within 12 hours of adhesion can predict lineage specification measured 14

days later. Consistent with such observations, studies with photoactive materials that can be either irreversibly softened [7] or stiffened [8] have revealed that the influence of ECM stiffness on MSC differentiation depends strongly on the initial duration of exposure to the stiffness cue. These approaches have introduced the concept that stem cells may possess "mechanical memory," such that initial exposure to instructive ECM stiffnesses for critical lengths of time shifts differentiation programs even when the ECM is subsequently softened [9].

Collectively, these observations raise the possibility that stem cells may be maximally primed within some temporal window to receive, remember, and act upon ECM stiffness inputs, and that a "point of no return" may exist beyond which stem cells no longer respond to these signals. However, a key limitation to definitively identifying the beginning and end points of these windows, and the molecular mechanisms that act therein, is the lack of a single ECM platform that can be reversibly stiffened or softened on cue. The absence of such materials represents a broad and important unmet need in the fields of stem cell engineering and mechanobiology.

Materials and Methods

Cell Culture

Adult rat NSCs were cultured as described previously [3, 10]. Briefly, cells were cultured in DMEM-F12 (Invitrogen, Carlsbad, California, USA) + N2 Supplement (Life Technologies, Carlsbad, California, USA) and 20 ng/mL FGF-2 on laminin-coated polystyrene plates. For differentiation experiments, cells were cultured in mixed differentiation medium (DMEM-F12 + N2, 1 μg/ml retinoic acid, 1% fetal bovine serum) if not otherwise noted.

Polyacrylamide Hydrogels

Nonswitchable polyacrylamide (PA) hydrogels were produced as described previously [4]. Briefly, acrylamide and bisacrylamide precursor solutions were degassed by nitrogen bubbling, and polymerized onto PlusOne Bind-Silane (GE Healthcare Life Sciences, Pittsburg, Pennsylvania, USA) treated glass coverslips with 0.1% ammonium persulfate and tetramethylethylenediamine. DNA gels were produced using sidearm and linker sequences as previously described [11-13]. The polymerization method was slightly optimized compared to the previously published method: Both sidearm sequences were added into the polymerization mix, and the solution was allowed to polymerize under degassing sonication for 15 minutes, before being mixed with linker DNA strand and pipetted onto Bind-Silane activated glass coverslips.

DNA/bis-crosslinked hydrogels were produced by adding additional acrylamide, bis-acrylamide, and APS/TEMED to the freshly combined DNA-acrydite-acrylamide polymer (final composition: 3.13% acrylamide and 0.008% bis reacted with 1mM hybridized SA1 + SA2 + L). For all gels, laminin functionalization was achieved by incubating gels in 50 μg/ml sulfo-SANPAH and irradiating with a UV flood lamp for 8 minutes. The gels were then washed once in PBS, and incubated with 20 μg/ml full length mouse laminin (EHS sarcoma derived) for 24 hours at 4°C.

Rheological Characterization

Rheological characterization of all hydrogels was performed using an Anton Paar (Ashland, Virginia, USA) Physica MCR 301 rheometer with an 8 mm parallel plate geometry. The solvent trap around the sample location was filled with water to prevent sample dehydration. The temperature of the sample was controlled by a Peltier element (Anton Paar).

Atomic Force Microscopy

Atomic force microscopy was performed on a Veeco (Bruker, Corporation, Camarillo, California, USA) Catalyst Bioscope instrument. All measurements of gel properties were done at room temperature in cell culture medium (DMEM-F12). The deflection sensitivity of each MLCT-BIO cantilever was measured against a glass cover slide, and the spring constant was determined by thermal tuning. Force-indentation curves were fitted against a Sneddon indentation model (cone indenting infinite half-space) to obtain elastic moduli [14].

Immunoblotting

Electrophoresis was performed using NuPAGE 4%-12% Bis-Tris Gels, and transfer to PVDF membranes for Western blotting was done in a tank blotting cell for 3 hours on ice. Primary antibody dilutions were 1:1,000. Horseradish-peroxidase conjugated secondary antibodies (Sigma-Aldrich, St. Louis, Missouri, USA) were used at 1:100,000 dilutions. Quantification was performed by imaging SuperSignal West Dura ECL substrate (Thermo-Fisher) in a Kodak Bio-Rad imager. Coimmunoprecipitation assays were prepared using a commercial kit (Pierce Classic Immunoprecipitation Kit) according to manufacturer's instructions. Briefly, cell lysates were pre-cleared against an agarose control resin, then incubated with 1% anti-β-catenin antibody (BD Biosciences, San Jose, California, USA. Product #610154) overnight. Antibody complexes were captured using a protein A/G resin and eluted in NuPage LDS sample buffer (Life Technologies).

Immmunofluorescence

Cells were fixed in 4% paraformaldehyde in PBS for 10 minutes. After washing thoroughly with PBS, cells were permeabilized and blocked with 0.3% Triton-X and 5% goat serum (room temperature, 1 hour). Thereafter, samples were incubated with primary antibodies for 24 hours at 4°C. After several washes, samples were incubated with secondary antibodies for 2 hours at room temperature. After two final washes, DAPI was added as a nuclear marker. Primary antibodies used were βIII-tubulin (Covance MMS-435P, Princeton, New Jersey, USA), GFAP (Abcam 7260, Cambridge, UK), Yes-associated protein (YAP; Cell Signaling, Danvers, Massachusetts, USA, Product #4912), β-catenin (BD 610154). Secondary antibodies from Life Technologies were obtained for the appropriate species conjugated with Alexa-488 and -546 dyes.

Viral Vectors

The rat YAP cDNA sequence was synthesized by IDT (Coralville, Iowa, USA) and inserted into a pCLPIT retroviral vector [4]. β-catenin reporter constructs (7xTFP) were used as described previously [15]. shRNA against YAP constructs (pLKO.1 vector system) were also obtained from Addgene. In all three cases, cell lines were established by selection with 1 ug/ml puromycin for 48 hours and 0.6 ug/ml puromycin thereafter.

YAP E66A and YAP S94A were generated via Quickchange PCR. YAP knockdown by shRNA was confirmed by Western blot (Supporting Information Fig. S3), and an 85% reduction of expression levels could be achieved in the high multiplicity of infection case.

Luciferase Assay

Cells were transfected with a 7xTCF luciferase reporter construct [16]. 105 cells per condition were lysed in 20 µl of lysis buffer (Promega, Sunnyvale, California, USA), mixed with 100 µl of Luciferase Assay substrate (Promega), and immediately measured in a luminometer (Promega TD 20/20).

DNA-Based Crosslinks Enable Dynamic Stiffness Modulation

As an initial, motivating study, we conducted serial adhesion experiments in which NSCs were first cultured on polyacrylamide (PA) ECMs of a given stiffness under media conditions that give rise to a mixture of neurons and glia (i.e., mixed differentiation—1 µM retinoic acid and 1% fetal bovine serum [10]), and then dissociated and reseeded on an ECM of a different stiffness. If NSCs were re-seeded onto a stiff ECM (72 kPa, 10% acrylamide and 0.3% bis) more than 3 days after initially being seeded on a soft ECM (0.7kPa, 4% acrylamide and 0.05% bis), the downstream lineage distribution matched that of cells cultured on soft substrates for the entire time course (Supporting Information Fig. S1). Conversely, cells cultured on stiff ECMs and then re-seeded onto soft ECMs exhibited lineage distributions characteristic of a soft ECM phenotype (i.e., high neurogenesis) only if the replating occurred earlier than 2 days in culture. These results began to bracket a critical temporal window of mechanosensitivity, where mechanical instruction of lineage commitment occurs no later than 2-3 days after initial adhesion. However, cell detachment induces the risk of disrupting cellular mechanosensing mechanisms that are linked to cytoskeletal organization as well as selecting for particular cellular subpopulations [17, 18]. We therefore sought to create a material system in which ECM stiffness could be dynamically and reversibly modulated without removing cells from the surface.

A mechanically-tunable ECM system capable of delivering temporally-defined stiffness cues to stem cells must meet several critical requirements: minimal swelling and contraction of the gel upon stiffening or softening to avoid cellular deformation, reversible stiffness modulation over a relevant stiffness range that encompasses stem cell mechanosensitivity to analyze the effects of temporal stiffening and softening on lineage specification, and functionalization with ECM adhesion proteins or peptides. Prior materials systems have met some but not all of these requirements. Several systems exhibit extensive swelling or shrinking upon stiffness-switching [11, 19-21], and photo-cleavable [22, 23] or photo-crosslinkable [8] gels are an advance, but their irreversible nature limits the scope of biological questions that can be asked.

We therefore engineered a PA ECM system based on prior PA hydrogels in which stiffness can be reversibly manipulated with oligonucleotide-based crosslinks [11, [20, 21]] (Fig. 1A). Two distinct, acrydite-functionalized DNA-oligonucleotides (“sidearms”) are copolymerized into a PA hydrogel, and subsequent addition of a soluble linker DNA strand (L) containing sequences complementary to the sidearms hybridizes with two sidearms and thereby adds additional crosslinks to stiffen the gel. Furthermore, the L strand also contains a “toehold” region that binds to neither of the sidearms, and thus subsequent addition of a “release strand” (R) that is fully complementary to L (including the toehold) can competitively hybridize with L to remove crosslinks and soften the gel (Fig. 1A). A further, critical innovation in this system is

that DNA crosslinks are formed via incubation of the two acrydite-functionalized DNA oligonucleotides with the linker strand to allow hybridization before their copolymerization into hydrogel. This enables substantially higher control over DNA crosslink concentrations than prior work and a much greater range of possible stiffness values [20, 21].

Figure 1

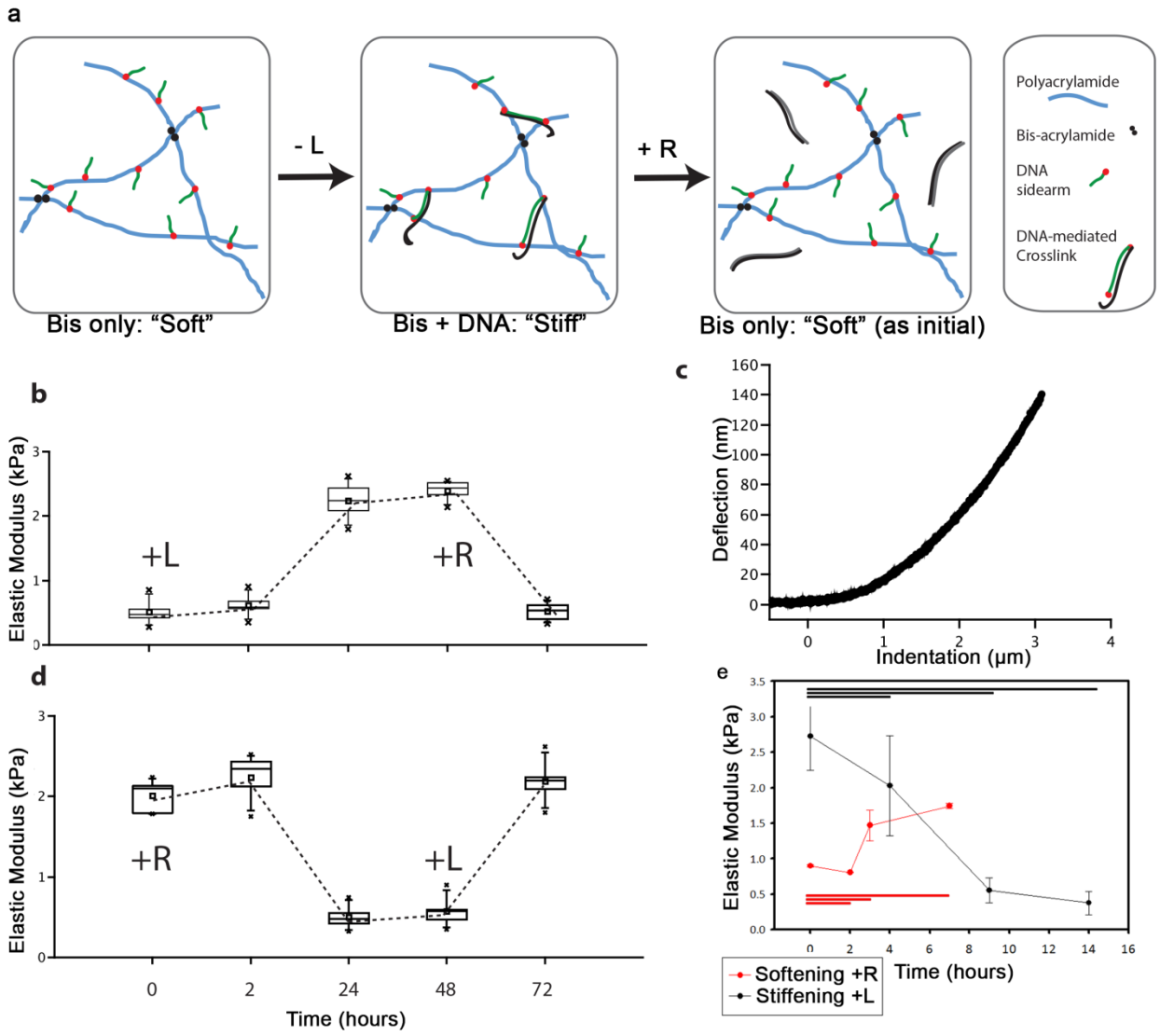

Figure 4: A DNA-bis crosslinked PA gel enabled dynamic and reversible modulation of stiffness. (A): Molecular schematic of DNA-bis-PA gels. PA-copolymerized with acrydite-DNA sidearms hybridize to a shared linker DNA-strand (L) to stiffen the gel. A release strand (R) can subsequently soften the gel by hybridizing to and removing L. (B–E): Atomic force microscopy (AFM) measurements of DNA-bis-PA gel stiffening (B). L strand was added at time 0 to DNA-bis-PA gels. AFM indentation measurements were conducted at various times, with a representative force curve illustrated in (C). At 48 hours, the R strand was added to induce softening. We observed softening to approximately the same stiffness value as at t = 0. Measurement of the analogous, reverse case of softening revealed similar behavior (D). The stiffening of the gel was followed in higher temporal resolution for the first 14 hours after addition of L strand, and a plateau was reached by 9 hours (E). B, D: box and whisker plots in this and subsequent figures represent a seven-number summary: square-mean, bar-median, box edges - 1 standard deviation,

whiskers - 95th and 5th percentile, x - min and max, n = 3. E - 1-way ANOVA, n = 3, error bars represent 1 standard deviation. Solid horizontal line represents $p < .05$ for connected color-corresponding points.

In such experiments involving a single, unidirectional change in stiffness, it is unclear whether the mechanical instruction of cell fate depends on the total time a differentiating cell is exposed to a given stiffness, the time point at which the stiffness is changed, or both. To distinguish among these possibilities, we took advantage of the reversibility of this material and performed stiffness and softness "pulse" experiments in which we were able to either transiently soften stiff gels by sequential addition of R and later L, or stiffen soft gels by addition of L and later R, at a range of times from 1 to 5 days after onset of differentiation (Fig. 2B). We found more β-III tubulin+ cells on the substrates that were soft within a 12-36 hour window versus later time windows, and less neuronal differentiation occurred when cells were exposed to stiff ECMs within this window. These results thus revealed that cells are most mechanosensitive and plastic during their first 12 to 36 hours of differentiation and become insensitive to stiffness changes (in either direction) once this mechanosensitive time window closes, narrowing the window significantly from our previous estimate of ~3 days.

Figure 2

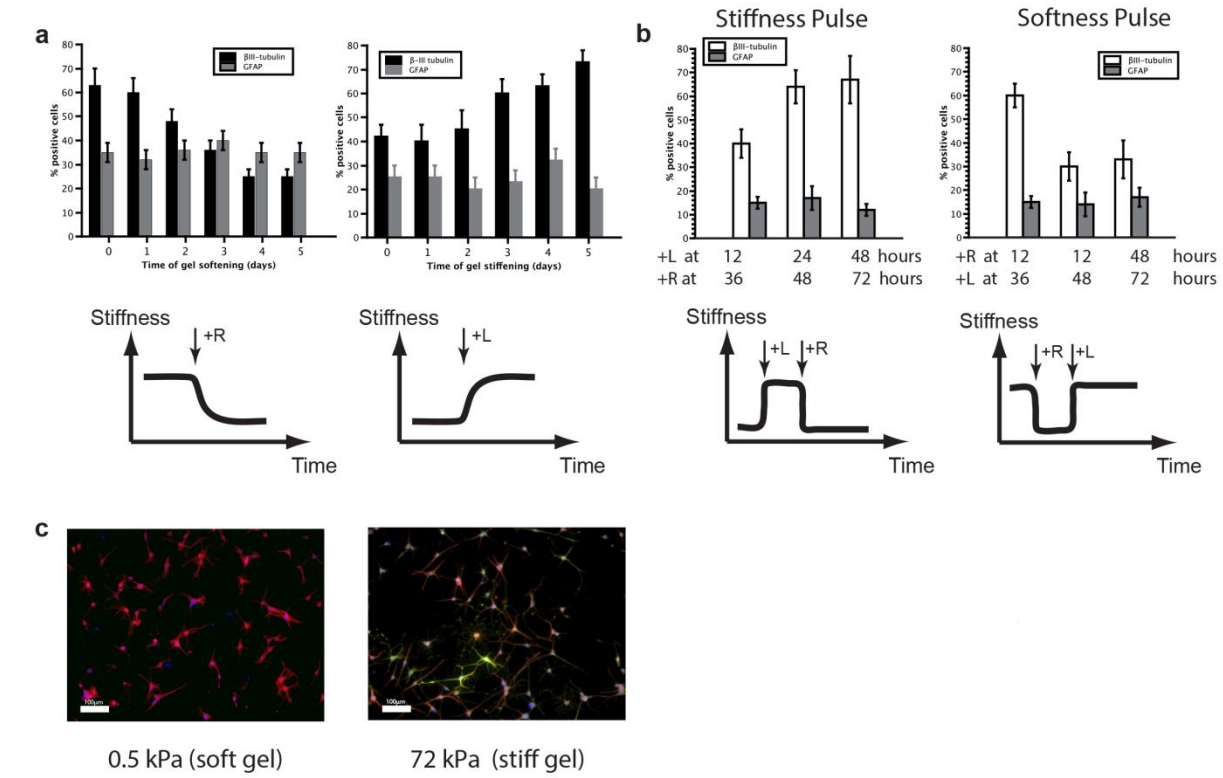

Figure 5: Changing stiffness of differentiating neural stem cells (NSCs) biased lineage commitment during the first two days after seeding. (A): NSC differentiation after dissociating cells from a PA gel and re-seeding on a new stiffness condition. (B): NSC differentiation under step-change stiffness conditions. NSCs were seeded on an initially stiff DNA-bis-PA gel, which was then softened after different intervals of time. Softening early increased the percentage of βIII-tubulin positive cells. However, there was no significant difference in lineage commitment if the substrate was softened later than 3 days after induction of differentiation. Error bars show 1 standard deviation, n = 3. (C): NSC differentiation under stiffness pulse conditions. DNA-bis-PA gels were seeded with NSCs, stiffened at 12-48 hours, then stiffened at 36-

72 hours, or in the converse case, NSCs were seeded on stiff gels, which were softened and thenlater stiffened from day 1 to day 5 after onset of differentiation. Mechanically instructed lineage commitment was plastic prior to 48 hours. Error bars show 1 standard deviation, n 5 3. (D): Representative images for neurogenesis on 300 Pa (soft) and 3kPa (stiff) gels (DAPI: Blue, βIII-tubulin: Red, GFAP: Green), scale bar: 100 μm.

The existence of a critical time window for mechanosensitive NSC differentiation raises the intriguing question of what molecular mechanisms are activated during this window and how they coordinate with signals traditionally understood to control NSC neurogenesis. The transcriptional coactivator YAP has previously been implicated as a regulator of a range of mechanosensitive behaviors, including mesenchymal stem cell differentiation, [18] where it functions as a molecular rheostat [9]. We first investigated whether total intracellular YAP levels depended on substrate stiffness and found levels substantially higher on stiff (75 kPa) versus soft (700 Pa) gels, in particular during the first 48 hours of differentiation (Fig. 3A, 3B).

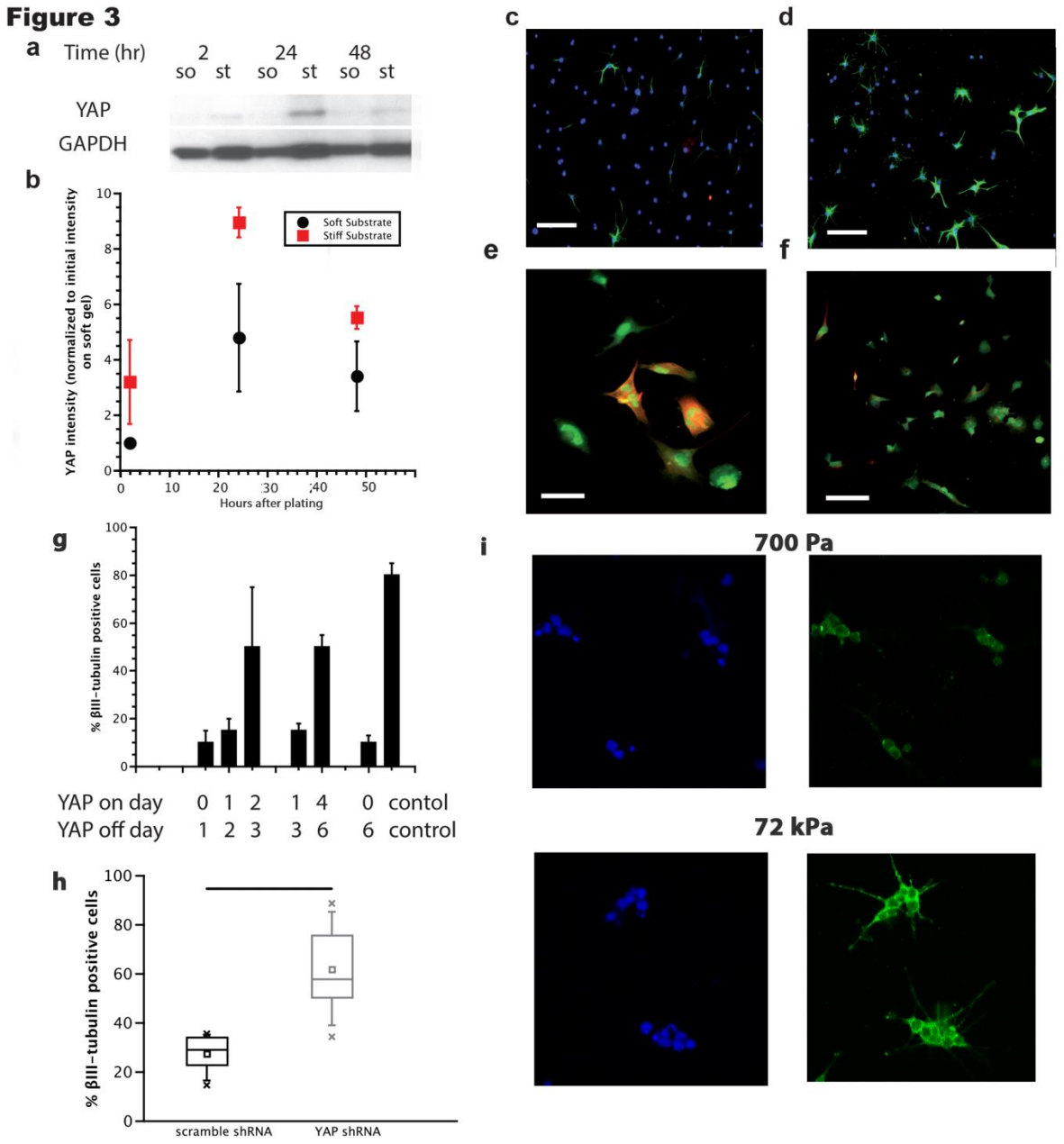

Figure 6: YAP dynamically varied with stiffness, and was necessary and sufficient for directing stiffness-mediated neurogenesis. (A, B): Western blot of total YAP following onset of differentiation. Total YAP levels showed a significant difference (B, normalized to initial YAP intensity on soft gel) on 700 Pa (soft) versus 75 kPa (stiff) gels. On stiff gels, relative levels of YAP were higher between 24 and 48hours, a period that corresponded with the mechanosensitive window described in Figure 2. Error bars represent 1 standard deviation, n = 3. Data is normalized to soft YAP intensity at 2 hours after plating. (C, D): shRNA knockdown of YAP. After 6 days of differentiation on laminin-coated tissue culture plastic, shRNA YAP knockdown (D) showed a higher ratio of βIII-tubulin positive cells than the control(C), quantified in (H) as a seven-number summary with n = 3, $p < .01$ 1-way ANOVA. DAPI: blue, βIII-tubulin: green. Scale bar: 100 µm.(E, F): YAP-GFP overexpressing NSCs on 700 Pa (E, soft) and 75 kPa (F, stiff) gels. DAPI: blue, bIII-tubulin: red, YAP-GFP: green. Scale bar: 100 µm. (G): Quantification of βIII-tubulin positive cells after pulsed YAP overexpression. Tetracycline was added to and withdrawn

from soft gel cultures at the indicated times. Cells that were exposed to increased YAP-GFP levels early in the differentiation process (day 0 and 1, day 1, and 2) were much less likely to commit to the neuronal lineage than cells that are exposed to YAP-GFP at later stages(day 2 and 3, or day 4, 5, 6), n 5 3, error bars represent 1 standard deviation, $p < 0.01$ 1-way ANOVA. (I): NSCs on both soft (top) and stiff (bottom) substrates showed no difference in the nuclear versus cytoplasmic localization of YAP. DAPI: blue, left. YAP: green, right, mean ratio ~0.3 N/C.

Given that matrix stiffness strongly regulates YAP expression, we next asked whether YAP may play a causal role in stiffness-mediated NSC lineage commimtent. To do this, we manipulated YAP levels by generating and expressing a YAP-GFP fusion construct (Supporting Information Fig. S3). First, under the same soft gel (0.7 kPa) differentiation conditions that had earlier supported robust neurogenesis in control NSCs (Fig. 2C), constitutive overexpression of YAP-GFP reduced neurogenesis (Fig. 3E, 3G). In contrast, when we suppressed YAP by transducing NSCs with a lentiviral vector carrying a previously validated anti-YAP shRNA [24], neurogenesis was strongly promoted, even on very stiff (72 kPa) substrates (Fig. 3C, 3D, 3F, 3G, 3H, Supporting Information Fig. S3). Thus, YAP is both necessary and sufficient to suppress neurogenesis, and manipulation of YAP expression can override stiffness regulation of lineage commitment.

Intriguingly, the mechanosensitive time window of 12-36 hours identified using ECM stiffness pulses (Fig. 2B) correlates closely with the observed YAP expression dynamics on stiff surfaces (Fig. 3A, 3B). To determine whether dynamic modulation of ectopic YAP expression (to emulate the YAP profile observed on stiff surfaces) could phenocopy the impact of stiffness on differentiation, we used a tetracycline-regulated gene expression system [25] that we introduced into a retroviral vector to mirror our stiffening/softening experiments by introducing pulses of YAP expression at critical time points throughout the lineage commitment process. We found that YAP-GFP overexpression exerted a particularly strong impact on lineage commitment early in differentiation (Fig. 3E, 3G). Specifically, YAP-GFP expression during day 1, day 2, or both days reduced neurogenesis to similarly low levels as if YAP-GFP were expressed during the whole 6-day differentiation window. These experiments implicate the same 12-36 hour window identified by both endogenous YAP expression in cells on a stiff substrate (Fig. 3B) and stiffness pulses introduced using the reversibly switchable gels (Fig. 2B).

With the knowledge that YAP is necessary and sufficient for mechanosensitive suppression of neurogenesis (Fig. 3), we next asked what mechanism drives this behavior. An obvious possibility based on previous studies with mesenchymal stem cells [18] would be that stiffness drives the nuclear translocation of YAP, which in turn may contribute to lineage commitment through YAP/TEAD coregulation of gene expression. Intriguingly, however, when we examined YAP localization via immunofluorescence, we did not observe differences in nucleo-cytoplasmic distribution as a function of matrix stiffness (Fig. 3I). Since YAP is regulated not only by expression levels and nuclear shuttling [18] but also by cytosolic interactions [26], we hypothesized that YAP could conceivably be functioning by interfacing with the transcriptional activity of other important signaling pathways. We thus investigated whether YAP could interact with effectors of neurogenesis. β-catenin is a critical component of the Wnt signaling pathway that plays critical roles in organismal development, stem cell differentiation, and cancer [15, 27-29], and we recently found that β-catenin is activated downstream of ephrin signaling to induce NSC differentiation [29]. Upon upstream signal activation, this protein translocates to the nucleus, where it acts as a transcriptional coactivator of

target genes, including the proneuronal transcription factor NeuroD1 in NSCs [30]. Interestingly, β-catenin has also been reported to bind to YAP within the Hippo signaling pathway, either directly or through coassociation with the β-catenin destruction complex [16, 26]. Thus, we hypothesized that YAP may sequester and thereby reduce β-catenin activity.

To investigate this possibility, we first asked if YAP expression had an effect on β-catenin transcriptional activity. Expression of a 7xTCF luciferase reporter [31] showed that overexpression of YAP yielded a sharp reduction in β-catenin transcriptional activity (Fig. 4A.) Addition of the GSK-3β inhibitor CHIR99021, which inhibits degradation of β-catenin and thereby potentiates its downstream signaling, significantly enhanced neuronal differentiation, and even rescued this differentiation in YAP-GFP overexpressing NSCs (Fig. 4B, 4C).

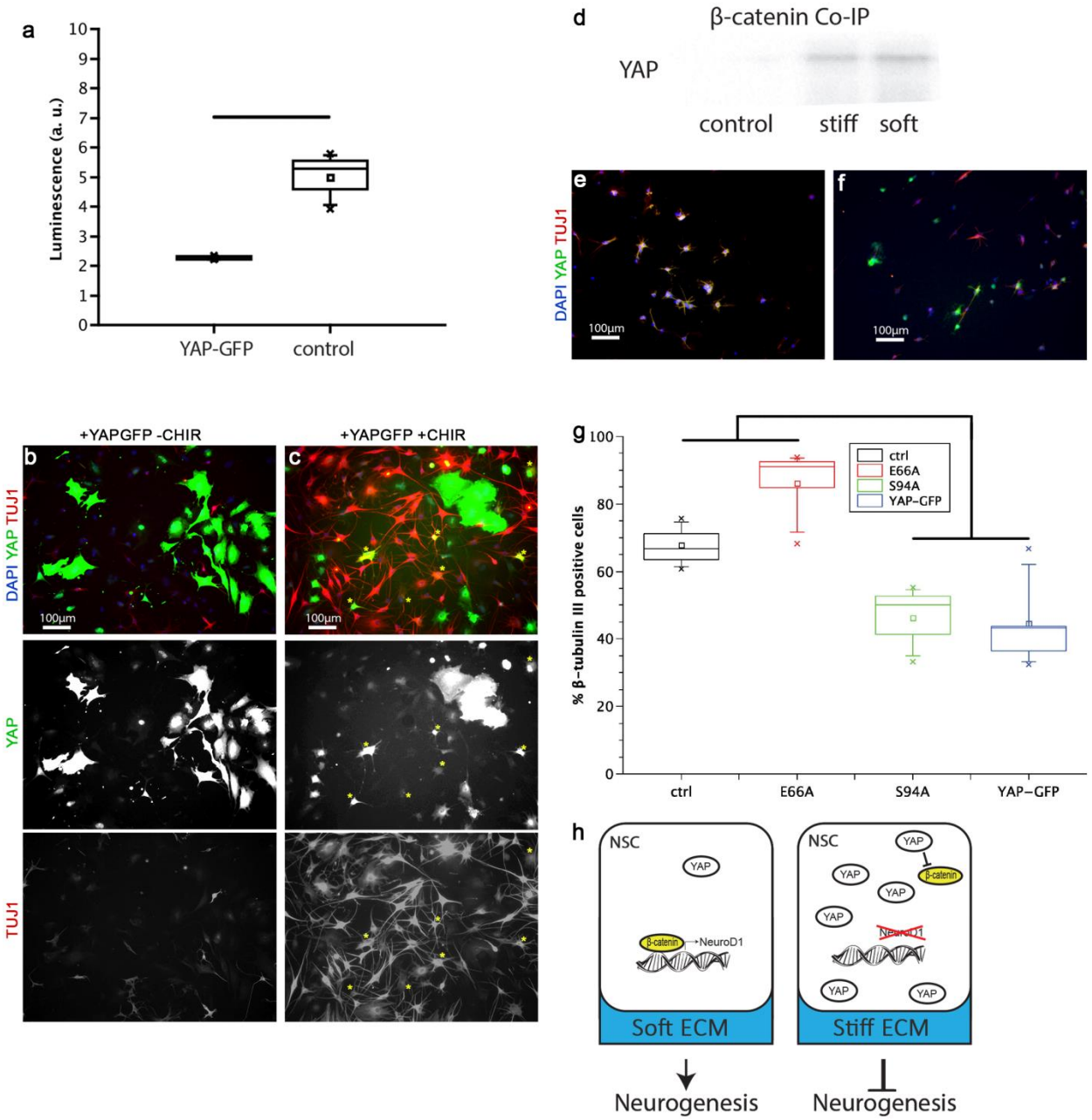

Figure 7: YAP interacted with b-catenin to bias stiffness-mediated NSC lineage commitment. (A): YAP-GFP decreased β-catenin transcriptional activity. The activity of a β-catenin responsive promoter-reporter was significantly reduced in YAP-GFP cells compared to con-trol cells (n 5 3, $p < .01$ by t-test). (B, C): In control cells (B), YAP-GFP cells did not stain positive for βIII-tubulin, but GSK3β inhibition by 3μM CHIR99021 treatment restored neural differentiation in some YAP-GFP cells (C). Yellow stars indicate cells that stain positive for both YAP-GFP and βIII-tubulin.(D): YAP and β-catenin interact in differentiating NSCs. Coimmunoprecipitation with a β-catenin antibody and probing with a YAP antibody showed that on both 300 Pa (soft) and 72 kPa (stiff) samples, YAP coprecipitated with β-catenin (control: no β-catenin antibody on stiff surface). (E, F): Binding mutants of YAP-GFP showed differentiation rescue of neurogenesis on soft (200 Pa) substrates. A YAP mutant unable to bind β-catenin (E66A) (E) showed the same level of neuronal differentiation as naïve, non-YAP expressing cells, compared to suppressed neurogenesis by YAP-GFP (compare with B). Numerous cells stained positive

for both βIII-tubulin and E66A YAP-GFP; in contrast, in the control YAP-GFP case there were no cells that stained positive for both βIII-tubulin and GFP. The S94A YAP mutant that lacked TEAD binding (F) suppressed neurogenesis to the same extent as wild type YAP-GFP (compare B). (G): Quantification of levels of neurogenesis in the naïve, E66A, S94A, and YAP-GFP cases. Naïve and E66A were significantly different from S94A and YAP-GFP cases on soft substrates (200 Pa) (n 5 3 gels, $p < .005$ by 1-way ANOVA). (H): Schematic of the proposed effect of substrate stiff-ness on NSC lineage commitment. On soft substrates, β-catenin drives transcription of neurogenesis effectors, such as NeuroD1. On stiffsubstrates, YAP levels are sufficiently high to sequester and inhibit available β-catenin, thereby preventing β-catenin dependent transcription.

The above results are consistent with a model in which YAP antagonizes β-catenin to suppress neural lineage commitment. To investigate whether these two molecules biochemically associate within NSCs, either by direct binding [26] or mutual association for example to Axin and the β−catenin destruction complex [26], we performed coimmunoprecipitation of β-catenin and YAP during the lineage commitment process (Fig. 4D). Pulldown of β-catenin and probing for YAP showed association between these two molecules on both very soft (200 Pa) and stiff (72 kPa) substrates. To investigate the functional consequences of YAP association with β-catenin, we performed loss-of-function studies in which we overexpressed a YAP mutant [24, 26] that lacks the ability to associate with β-catenin (YAP-E66A). In parallel, a YAP mutant unable to bind TEAD proteins (YAP-S94A) [26] was investigated to assess the direct transcriptional role of YAP. Interestingly, the YAP-E66A mutant, whose interaction with β-catenin is ablated, exhibited similar, high neurogenesis on soft substrates as control cells not expressing YAP (Fig. 4E, 4G). In contrast, YAP-S94A overexpressing cells exhibited similar, low levels of neuronal differentiation as NSCs overexpressing wild type YAP (Fig. 4F, 4G). This result indicates that YAP's β-catenin binding activity plays a much stronger functional role in NSC mechanoregulation than YAP's transcriptional coregulatory activity. This is fundamentally distinct both from previous observations in MSCs and the nuclear and TEAD-mediated mechanism of action classically portrayed in the Hippo pathway. Therefore, we propose a model wherein matrix stiffness controls neurogenesis by regulating a balance between pro-neurogenic β-catenin activity and anti-neurogenic YAP activity, an antagonism that depends primarily on a direct binding interaction between β-catenin and YAP (Fig. 4H).

Discussion

In this study, we have identified a 12-36 hour mechanosensitive time window during which NSC lineage commitment is maximally receptive to ECM stiffness inputs. In particular, by leveraging a material platform in which stiffness can be dynamically modulated, we found that exposure to a transient stiffness pulse from 12 to 36 hours was sufficient to suppress neurogenesis on soft matrices, and conversely a “softness pulse” during this same time window rescued neurogenesis on stiff matrices. Furthermore, we identified signaling events that mediate the impact of these stiffness cues on stem cell differentiation. Endogenous expression of the transcriptional coactivator YAP peaked during the 12-36 hour time window, and ectopic, pulsed overexpression of YAP during this window was sufficient to override soft matrix cues and thereby block neuronal differentiation. However, counter to the proposed model of YAP regulation in stiffness-dependent differentiation of mesenchymal stem cells, stiffness did not lead to nuclear versus cytoplasmic partitioning of YAP. Furthermore, YAP coprecipitated with the pro-neurogenic effector β-catenin, and disruption of this interaction reversed YAP-mediated suppression of neurogenesis. Analogously, pharmacological activation of β-catenin restored NSC

neurogenic lineage commitment even with YAP overexpression. Our results therefore support a model in which matrix stiffness acts during a critical time window to regulate a balance between Wnt/β-catenin versus YAP signaling, whereby YAP antagonizes the neurogenic effects of β-catenin through a binding interaction. This model is compatible with direct binding and sequestration of β-catenin [24], or suppression of β-catenin through association of both of these proteins with Axin within the β-catenin destruction complex [16, 32]. Further resolution of the precise mechanism of this interaction, and of the temporal dynamics of the balance between YAP and β-catenin during the critical time window, represent intriguing future possibilities for investigation.

A critical innovation and enabling technology in this study was the utilization of bis-acrylamide/oligonucleotide PA hydrogels in which stiffness could be dynamically and reversibly modulated. The underlying covalent crosslinks provide a basal structural stability (also reducing shrinking/swelling), on top of which the fully reversible DNA hybridization crosslinks can dynamically and reversibly modulate stiffness on a timescale that enables investigation of stem cell lineage commitment (Fig. 1E). Hydrogel materials in which stiffness can either be irreversibly increased [8] or decreased [7] using photoirradiation have been previously employed to investigate stem cell lineage commitment; however, a two-way mechanical switch in which stiffness may repeatedly increased and/or decreased was a key advance that enabled us to define a critical window during which lineage commitment is maximally sensitive to mechanical inputs. Our work also suggests that the specific temporal window of exposure to a defined stiffness cue beginning and ending at specific times, rather than the duration of exposure, governs lineage decisions. Stiffness step changes that occurred before the window opened (<24 hours after seeding) did not bias differentiation strongly, but pulsed stiffnesses of the same duration (24 hours) inside of the window strongly influenced fate distributions. Isolation of this defined temporal window enabled us to connect these changes with time-dependent signaling events and thus offer a mechanistic model for mechanosensitive differentiation. Importantly, these materials are uniquely well suited to interrogate a low-stiffness regime (0.1–10 kPa), which corresponds well to the elasticity of hippocampal tissue [12] and may be of value for investigating lineage commitment in other soft tissues. With additional tuning to reduce DNA exclusion and to promote DNA (e.g., shortened oligos or smaller gels) diffusion into the gel, stiffer regimes could even further broaden the range of stem cell and mechanobiology investigations enabled by this system.

Conclusion

In this study, we have shown that NSCs are maximally sensitive to mechanical inputs from 12-36 hours after the introduction of soluble differentiation cues, and become insensitive to further changes in the elastic modulus of their microenvironment after this window closes. These findings were enabled by further innovation of a polyacrylamide gel whose stiffness can be dynamically and reversibly controlled by addition of DNA oligonucleotides. We subsequently correlated this time window with increased expression of the transcriptional co-activator YAP, and implicated YAP as the messenger of mechanical cues from the extracellular matrix. Overexpression of YAP specifically during this time window was sufficient to override soft matrix cues and suppress neurogenesis, while silencing of YAP ablated the ability of stiff microenvironments to suppress neurogenesis. However, we observe that YAP does not exhibit mesenchymal-like changes in nuclear translocation in response to stiffness cues, and we link YAP's capacity to block neuronal differentiation to an inhibitor interaction with β-catenin. Our

data thus support a model where a protein protein-level interaction between YAP and β-catenin independent of nuclear translocation is responsible for transducing mechanical cues to NSC differentiation programs. Our study thereby advances our mechanistic understanding of the temporal and proteomic control of stem cell differentiation, as well as indicates possible regulatory interactions between Hippo and Wnt signaling.

Acknowledgments

We gratefully acknowledge the California Institute for Quantitative Biosciences and the California Institute for Regenerative Medicine for their support through the CIRM/QB3 Shared Stem Cell Facility. This work was supported by a grant from the NIH (1R01NS074831 to D.V.S. and S.K.) as well as fellowships from the Human Frontier Science Program (S.R.) and the NSF (K.G.) We thank John Wiley & Sons, Inc. for permission to republish work originally published in: "Dynamics of Mechanosensitive Neural Stem Cell Differentiation," Stem Cells, 2017;35:497–506 by Sebastian Rammensee, Michael S. Kang, Katerina Georgiou, Sanjay Kumar, and David V. Schaffer.

References

1. Engler, A. J., Sen, S., Sweeney, H. L. & Discher, D. E. Matrix elasticity directs stem cell lineage specification. *Cell* **126,** 677–689 (2006).
2. Gilbert, P. M. *et al.* Substrate elasticity regulates skeletal muscle stem cell self-renewal in culture. *Science* **329,** 1078–81 (2010).
3. Saha, K. *et al.* Substrate Modulus Directs Neural Stem Cell Behavior. *Biophys. J.* **95,** 4426–4438 (2008).
4. Lim, D. A., Huang, Y.-C. & Alvarez-Buylla, A. The adult neural stem cell niche: lessons for future neural cell replacement strategies. *Neurosurg. Clin. N. Am.* **18,** 81–92, ix (2007).
5. Keung, A. J., de Juan-Pardo, E. M., Schaffer, D. V & Kumar, S. Rho GTPases mediate the mechanosensitive lineage commitment of neural stem cells. *Stem Cells* **29,** 1886–97 (2011).
6. Elkin, B. S., Azeloglu, E. U., Costa, K. D. & Morrison, B. Mechanical heterogeneity of the rat hippocampus measured by atomic force microscope indentation. *J. Neurotrauma* **24,** 812–22 (2007)
7. Moore, S. W., Roca-Cusachs, P. & Sheetz, M. P. Stretchy Proteins on Stretchy Substrates: The Important Elements of Integrin-Mediated Rigidity Sensing. *Dev. Cell* **19,** 194–206 (2010).
8. Fu, J. *et al.* Mechanical regulation of cell function with geometrically modulated elastomeric substrates. *Nat. Methods* **7,** 733–6 (2010).
9. Yang, C., Tibbitt, M. W., Basta, L. & Anseth, K. S. Mechanical memory and dosing influence stem cell fate. *Nat. Mater.* (2014). doi:10.1038/nmat3889
10. Guvendiren, M. & Burdick, J. A. Stiffening hydrogels to probe short- and long-term cellular responses to dynamic mechanics. *Nat. Commun.* **3,** 792 (2012).
11. Peltier, J., Agrawal, S., Robertson, M. J. & Schaffer, D. V. In vitro culture and analysis of adult hippocampal neural progenitors. *Methods Mol. Biol.* **621,** 65–87 (2010).
12. Aragona, M. *et al.* A mechanical checkpoint controls multicellular growth through YAP/TAZ regulation by actin-processing factors. *Cell* **154,** 1047–59 (2013).
13. Dupont, S. *et al.* Role of YAP/TAZ in mechanotransduction. *Nature* **474,** 179–183 (2011).

14. Previtera, M. L. *et al.* Fibroblast morphology on dynamic softening of hydrogels. *Ann. Biomed. Eng.* **40,** 1061–72 (2012).
15. Lin, D. C., Yurke, B. & Langrana, N. A. Inducing reversible stiffness changes in DNA-crosslinked gels. *J. Mater. Res.* **20,** 1456–1464 (2005).
16. Jiang, F. X., Yurke, B., Firestein, B. L. & Langrana, N. A. Neurite outgrowth on a DNA crosslinked hydrogel with tunable stiffnesses. *Ann. Biomed. Eng.* **36,** 1565–1579 (2008).
17. Lin, D., Yurke, B. & Langrana, N. A. Mechanical Properties of a Reversible, DNA-Crosslinked Polyacrylamide Hydrogel. *J. Biomech. Eng.* **126,** 104 (2004).
18. Kloxin, A. M., Tibbitt, M. W. & Anseth, K. S. Synthesis of photodegradable hydrogels as dynamically tunable cell culture platforms. *Nat. Protoc.* **5,** 1867–87 (2010).
19. Kloxin, A. M., Kasko, A. M., Salinas, C. N. & Anseth, K. S. Photodegradable Hydrogels for Dynamic Tuning of Physical and Chemical Properties. *Science (80-.).* **324,** 59–63 (2009).
20. Zhao, B. *et al.* TEAD mediates YAP-dependent gene induction and growth control. *Genes Dev.* **22,** 1962–71 (2008).
21. MacKay, J. L., Keung, A. J. & Kumar, S. A Genetic Strategy for the Dynamic and Graded Control of Cell Mechanics, Motility, and Matrix Remodeling. *Biophys. J.* **102,** 434–442 (2012).
22. Imajo, M., Miyatake, K., Iimura, A., Miyamoto, A. & Nishida, E. A molecular mechanism that links Hippo signalling to the inhibition of Wnt/β-catenin signalling. *EMBO J.* **31,** 1109–22 (2012).
23. Anastas, J. N. & Moon, R. T. WNT signalling pathways as therapeutic targets in cancer. *Nat. Rev. Cancer* **13,** 11–26 (2013).
24. Niehrs, C. The complex world of WNT receptor signalling. *Nat. Rev. Mol. Cell Biol.* **13,** 767–79 (2012).
25. Ashton, R. S. *et al.* Astrocytes regulate adult hippocampal neurogenesis through ephrin-B signaling. *Nat. Neurosci.* **15,** 1399–406 (2012).
26. Bugaj, L. J., Choksi, A. T., Mesuda, C. K., Kane, R. S. & Schaffer, D. V. Optogenetic protein clustering and signaling activation in mammalian cells. *Nat. Methods* **10,** 249–52 (2013).
27. Kuwabara, T. *et al.* Wnt-mediated activation of NeuroD1 and retro-elements during adult neurogenesis. *Nat. Neurosci.* **12,** 1097–105 (2009).
28. Cai, J., Maitra, A., Anders, R. a, Taketo, M. M. & Pan, D. β -Catenin destruction complex- independent regulation of Hippo – YAP signaling by APC in intestinal tumorigenesis. *Genes Dev.* 1–14 (2015).
29. Fuerer, C. & Nusse, R. Lentiviral vectors to probe and manipulate the Wnt signaling pathway. *PLoS One* **5,** e9370 (2010).
30. Azzolin, L. *et al.* YAP/TAZ Incorporation in the β-Catenin Destruction Complex Orchestrates the Wnt Response. *Cell* **158,** 157–70 (2014).
31. Chippada, U., Yurke, B. & Langrana, N. A. Simultaneous determination of Young's modulus, shear modulus, and Poisson's ratio of soft hydrogels. *J. Mater. Res.* **25,** 545–555 (2010).
32. Liedl, T., Dietz, H., Yurke, B. & Simmel, F. Controlled trapping and release of quantum dots in a DNA-switchable hydrogel. *Small* **3,** 1688–93 (2007).
33. Butt, H.-J., Cappella, B. & Kappl, M. Force measurements with the atomic force microscope: Technique, interpretation and applications. *Surf. Sci. Rep.* **59,** 1–152 (2005).

Supplementary Information

Gel	E (kPa)	G' (kPa)	G" (kPa)	% AA	% Bis	DNA (mM)	Laminin (ng/mL)
Soft (AA-Bis)	0.2	0.072	0.005	4	0.05	0	20
Stiff (AA-Bis)	72	14	.01	10	0.3	0	20
DNA (AA-Bis-DNA)	3 - 0.3	~1.1	~0.9	3.13	0.008	1	20

Supplementary Table S1: E is measured by atomic force microscopy (Fig. 2.1b, d). G' and G" is measured by parallel plate rheometry (new measurements, Supplementary Figure S2). DNA concentration is the concentration of S1+S2+L used in co-polymerization reaction. Swelling ratio is ratio of hydrated gel after polymerization and after 2 days equilibriation in PBS. Laminin concentration corresponds to the concentration of full length EHS sarcoma purified laminin reacted with sulfo-SANPAH.

Supplementary Figure S1

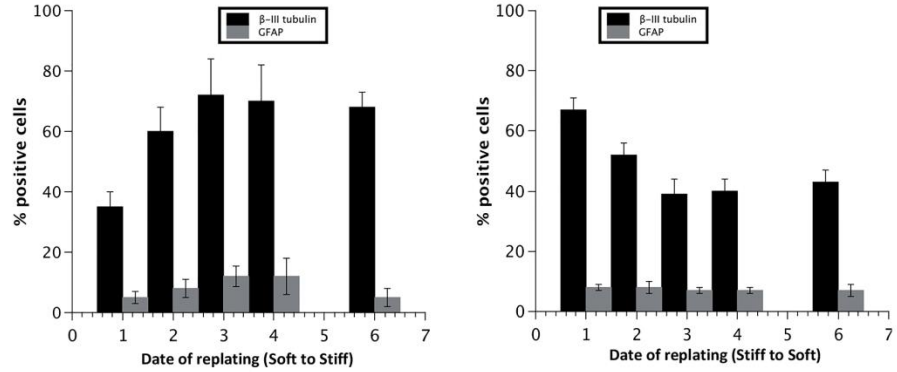

Supplementary Figure S2

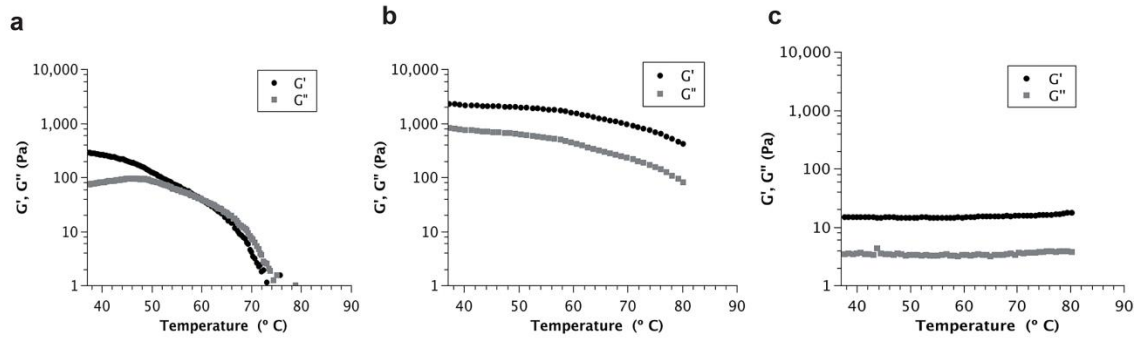

Supplementary Figure S3

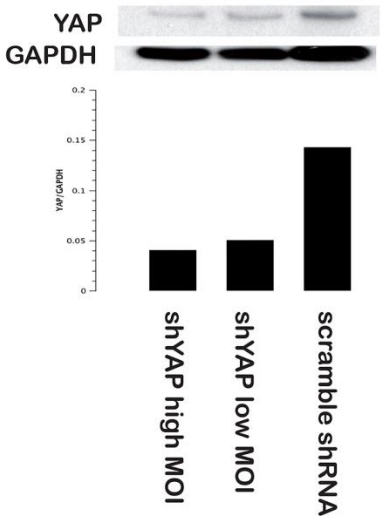

Figure S1: Replating cells from soft to stiff and vice versa shows that they were susceptible to the stiffness of the environment predominantly in early timepoints. On the horizontal axis, the day of replating is shown, and on the vertical axis the percentage of marker-positive cells is shown. The earlier the cells are replated (day 1-2), the closer their population of neurons matches the day 6 control (always at final stiffness). Error bars represent 1 standard deviation, n=3.

Figure S2: Temperature-dependent rheology of DNA-crosslinked PA gels. To characterize elastic behavior of a DNA-only crosslinked gel (DNA-PA), shear rheometry was performed over a temperature range spanning the predicted denaturation (melting) temperature of these DNA crosslinks (Figure S1 A,B,C). DNA-PA gels crosslinked purely by DNA oligomers turned completely fluid at temperatures over 70 °C (Figure S1A), indicated by the crossover of the storage modulus and the loss modulus. In contrast, DNA-Bis-PA gels significantly softened but did not liquefy upon heating (Figure S1B). Polyacrylamide-Bis gels (Figure S1C) showed no temperature-dependent change in stiffness.

Figure S3: Western blot and quantification of shRNA knockdown of YAP. The high MOI shYAP was used for all experiments. The lanes of the gel correspond to the quantification below.

Chapter 4: Interactions of YAP and β-catenin in Neural Stem Cell Differentiation.

Abstract

The ability of matrix properties, such as elastic modulus, to influence stem cell behavior and differentiation is increasingly appreciated. However, many of the specific biochemical interactions that propagate from stiffness inputs are poorly understood. Previous work from our groups has identified the signaling intersection of Hippo and Wnt via YAP and β-catenin as critical for mechanosensitive stem cell differentiation, but the nature of this interaction is still contentious. To help elucidate the intersection of these two pathway effectors, we analyzed YAP's subcellular localization and biochemical co-association in hippocampal neural stem cells. We report that the localization of YAP has a strong impact on both its ability to suppress neurogenesis and its ability to bind to beta-catenin, with nuclear YAP being strongly neurosuppressive and cytoplasmic YAP being neurogenic. We thereby propose a model in which YAP's ability to negatively regulate beta-catenin within NSCs is limited to the nucleus, and where cytoplasmic YAP does not inhibit β-catenin transcriptional activity. These findings thus demonstrate a novel, biochemical explanation for YAP's strong stiffness-dependent nuclear vs cytoplasmic localization, the hallmark of its mechanotransductive activity.

Introduction

Neural stem cell (NSC) differentiation is a process than continually generates new neurons, astrocytes, and oligodendrocytes in the mammalian brain throughout life. NSCs integrate an array of multifaceted and highly organized extracellular signals, such as paracrine and juxtacrine factors, into coordinated fate decisions through various signaling cascades. Of these, the influence of mechanical properties such as substrate elastic modulus, have recently begun to be appreciated as an important factor in influencing fate specification. However, the molecular pathways that underlie mechanosensing add an extra dimension of complexity on top of an already interwoven and complex network of signaling pathways.

Of these various pathway proteins, one that has garnered recent interest is the transcriptional coactivator Yes-associated protein 1 (YAP or YAP1). YAP was first reported as a potent oncogene and as the main effector of the Hippo signaling pathway. Normal YAP expression is associated with upregulating cell cycle and proliferation, and inhibition of YAP via the Hippo pathway is critical for cell-contact inhibition and control of organ size[1]. This occurs through phosphorylation of YAP by the tumor suppressor genes LATS1/2 and subsequent association with 14-3-3 proteins in the cytoplasm, where YAP is eventually ubiquitinated by β-TRCP and degraded[2]. When YAP is transcriptionally active, it translocates from the cytoplasm to the nucleus, where it is able to drive a variety of transcriptional programs through association with transcriptional coactivators such as TEAD1-4[3] and Runx2[4], which in turn are associated with stem cell maintenance and differentiation[5].

However, YAP has also recently been described as a potent mechanotransducer, where nuclear / cytoplasmic localization is regulated by substrate stiffness, with stiff substrates promoting nuclear localization and soft ones enhancing cytoplasmic localization[6]. Interestingly, this mechanism appears to occur in a Hippo-independent manner, as knockout of LATS1/2 is insufficient to block stiffness-specific localization[7]. Indeed, answering how signaling information reaches and is integrated and relayed by YAP is an ongoing and active field of inquiry, with candidate upstream regulators including Rho GTPases[6], angiomotin[8], and F-actin

capping proteins[7]. YAP itself also crosstalks with over various signaling pathways, such as PI3K-Akt[9] or Wnt[10–12].

Previous work in our lab has implicated the Wnt-Hippo signaling axis as an important mechanism through which stiffness-mediated YAP activation leads to suppression of neurogenesis[13]. In NSCs, stiff substrates lead to an accumulation of YAP and a corresponding suppression of β-catenin signaling activity. As Wnt signaling is known to regulate NSC neurogenesis[14], and because YAP has been shown to have suppressive effects on β-catenin activity[11,12], we hypothesized that this was the mechanism by which YAP enacted its neurosuppressive effects. However, the literature is not in consensus regarding the mechanism by which YAP and β-catenin interact, and it has become increasingly clear that these signaling nodes serve as integration points rather than simple connections. For example, one proposed model is that phosphorylated YAP is capable of directly binding to and sequestering β-catenin from interfacing with TCF transcription factors, thereby inhibiting its activity[12]. Another study has demonstrated that YAP is involved in the canonical Wnt pathway, and performs an integral role in β-catenin modulation by being a component of the Axin-APC-GSK3β destruction complex. In this model, YAP binds to Axin1 and recruits the ubiquitin ligase β-TrCP to mark β-catenin for degradation in cytoplasm. Further complicating the picture are recent reports suggesting that YAP itself is regulated by components of the destruction complex[15]. Cai and colleagues report that APC, a component of the destruction complex, can act as a scaffolding protein for Salvador and Lats1, which are both canonical Hippo signaling components, and regulate deactivation and turnover of YAP. Many of these additional reports also focus on canonical signal transduction via Wnt and the Hippo core kinases, rather than inputs from cytoskeletal elements.

The confluence of many proposed interaction models in addition to the relatively modest level of inquiry in YAP-β-catenin mechanotransduction, we began probing unresolved questions after our prior study – though our intial study implicated YAP as the main messenger and transducer of mechanical inputs from the ECM, the localization phenotype did not match previously published observations. Specifically, YAP localization in NSCs is strikingly insensitive to substrate modulus, with a constant level of nuclear vs cytoplasmic localization in all stiffness conditions (~0.6 N/C). This raised the possibility that YAP's ability to suppress β-catenin was occurring through another, localization-independent mechanism. For example, it has been suggested that phosphorylated YAP is capable of suppressing β-catenin activity regardless of cytoplasmic localization[12], and that YAP phosphorylation dictates whether its effects support β-catenin activity, in the case where unphosphorylated YAP acts to facilitate β-catenin nuclear transport[16]. The question of how YAP phosphorylation and subcellular localization impact its effects on Wnt signaling is thus still only partially answered, despite being a critical component of mechanosensitive NSC differentiation. We thus decided to use genetic perturbations of YAP expression in NSCs to further determine how YAP signals to β-catenin in the context of stiffness-sensitive neurogenesis.

Methods

Cell Culture

Adult rat NSCs were cultured as described previously (Saha, 2011). Briefly, cells were cultured in DMEM-F12 (Invitrogen, Carlsbad, California, USA) + N2 Supplement (Life Technologies, Carlsbad, California, USA) and 20 ng/mL FGF-2 on laminin-coated polystyrene plates. For differentiation experiments, cells were cultured in mixed differentiation medium (DMEM-F12 + N2, 1 μg/ml retinoic acid, 1% fetal bovine serum) if not otherwise noted.

Polyacrylamide Hydrogels

Polyacrylamide (PA) hydrogels of varying stiffness were produced as described previously (Keung, 2011). Briefly, acrylamide and bisacrylamide precursor solutions were degassed by nitrogen bubbling, and polymerized onto PlusOne Bind-Silane (GE Healthcare Life Sciences, Pittsburg, Pennsylvania, USA) treated glass coverslips with 0.1% ammonium persulfate and tetramethylethylenediamine. Laminin functionalization, which is necessary for NSC survival and attachment, was achieved by incubating gels in 50 μg/ml sulfo-SANPAH and irradiating with a UV flood lamp for 8 minutes. The gels were then washed once in PBS, and incubated with 20 μg/ml full length mouse laminin (EHS sarcoma derived) in PBS for 24 hours at 4°C.

Immmunofluorescence

Cells were fixed in 4% paraformaldehyde in PBS for 10 minutes. After washing thoroughly with PBS, cells were permeabilized and blocked with 0.3% Triton-X and 5% goat serum (room temperature, 1 hour). Thereafter, samples were incubated with primary antibodies for 24 hours at 4°C at 1% goat serum. After several washes, samples were incubated with secondary antibodies for 2 hours at room temperature. After two final washes, DAPI was added as a nuclear marker for 15 minutes, and then the coverslips were transferred to fresh PBS for imaging. Primary antibodies used were βIII-tubulin (Covance MMS-435P, Princeton, New Jersey, USA), GFAP (Abcam 7260, Cambridge, UK), Yes-associated protein (YAP; Cell Signaling, Danvers, Massachusetts, USA, Product #4912), β-catenin (BD 610154). Secondary antibodies from Life Technologies were obtained for the appropriate species conjugated with Alexa-488, -546, and -647 dyes. Images were acquired using a Prairie Systems swept field laser scanning confocal.

Cloning

Generation of SV40-NLS tagged YAP-VENUS and HIV-REV tagged YAP-VENUS was accomplished through PCR. C-terminal fusions were created using the following primers:
pr_YAP3SV40: AACCTTTCGCTTCTTTTTAGGTAACCACGTGAGAAAGCTTTCTTTA TCT,
pr_YAP3REV: ATCAAGAGTAAGTCTCTCAAGCGGTGGTAGTAACCACGTGAGAAAG CTTTCTTTATCT, and
pr_YAP5F: TAGGTTTAAACGGATCCACTAGTTCTAGAG. The resulting PCR product was digested with SfiI and PmeI for 1 hour at 37°C then 1 hour at 50°C and purified by Qiagen PCR cleanup column. These fragments were then ligated into the pCLPIT tet-OFF backbone (Saha, 2011) and verified by sequencing.

The S94A-YAP construct was previously synthesized by M. Kang as described previously[13].

Viral Vectors

Retrovirus production was accomplished using the pCLPIT tet-OFF system. HEK 293Ts were cultured on a 15cm polystyrene plate in Iscove's Modified Eagle Medium (IMDM) with 10% FBS and 1% penicillin-streptomycin until 90% confluency. 30μg of transfer plasmid, 12μg of pCMV gag-pol, and 8μg of pcDNA3 IVS VSV-G were incubated with PEI for 10 minutes in PBS, then dispersed into the plate and swirled. After two and three days, the media was collected and replaced with fresh supplemented IMDM, and purified by ultrafugation through a 20% sucrose gradient. Cell lines were established by infection at a 0.5 MOI and selected in 0.6 ug/ml puromycin for four days. Cell lines were maintained in 100ng/mL doxycycline during culture to repress YAP expression, due to the observation that prolonged expression of transgene lead to differentiation. Dox repression was relieved 24 hours before the initiation of differentiation experiments, after seeding onto polyacrylamide gels.

Results

C-Terminal Fusion of Localization Tags efficiency directs YAP localization

We began by asking the following question: if NSCs do not show robust localization of YAP constructs to nucleus or cytoplasm in response to stiffness, is the pathway by which YAP activity suppresses neurogenesis similarly insensitive to subcellular localization? To answer this, we created mutations of YAP-VENUS with C-terminal localization tag fusions (Figure 1). A nuclearly localizing YAP-VENUS-SV40NLS (YGFP-NLS) and a cytoplasmically localizing YAP-VENUS-HIV_REV_NES (YGFP-NES) were synthesized. In addition, we used a previously synthesized S94A mutated YAP that is deficient in TEAD binding[13] as a control, in addition to pCLPIT-VENUS.

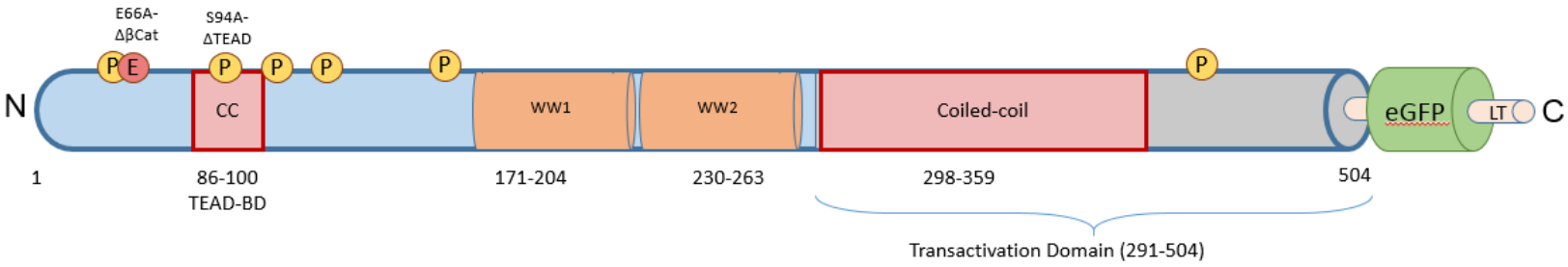

Figure 8: Schematic of YAP mutants. CC – Coiled-coil domain, LT – Localization tag. NLS-YAP variants were generated with LT = SV40 large T antigen tag (PKKKRKV). NES-YAP variants were generated with LT = HIV REV-NES tag (LPPLERLTLD). S94A-YAP is deficient in TEAD-binding. LATS1/2 phosphorylation sites are marked.

Expression of these constructs in NSCs lead to robust nuclear/cytoplasmic partitioning and localization (Figure 2A). YGFP-NLS cells showed strong nuclear localization of exogenous YAP (shown by GFP expression), though there appeared to be some level of saturation (Figure 2A). Low to moderate levels of YGFP-NLS expression lead to strong nuclear localization, but very high levels lead to "bleeding" throughout the rest of the cell. Similarly, YGFP-NES expression leads to robust cytoplasmic localization (Figure 2A,B). In the YGFP-NES cells, verification of nuclear export is difficult, but z-stacking through the colonies of cells clearly demonstrates that that GFP expression is localized outside of cellular nuclei (Figure 2B). Again, there appeared to be a saturation effect in the YGFP-NES cells, where low to moderate levels of expression showed robust cytoplasmic localization, but higher levels of expression showed increased enrichment in nucleus and cytoplasm both.

Nuclear localization of YAP suppresses neurogenesis, while nuclear export may enhance it

With the expression and localization phenotypes of these cells validated, we next examined whether or not they exhibited changes in the levels of neurogenesis on soft substrates. We seeded cells onto polyacrylamide gels as previously described[17,18] at low elastic modulus (~700 Pa), relieved dox suppression of YAP expression, and differentiated cells for 6 days and stained for lineage markers. We hypothesized that if YAP and β-catenin were interacting in a direct, phosphorylation and destruction complex independent mechanism, that

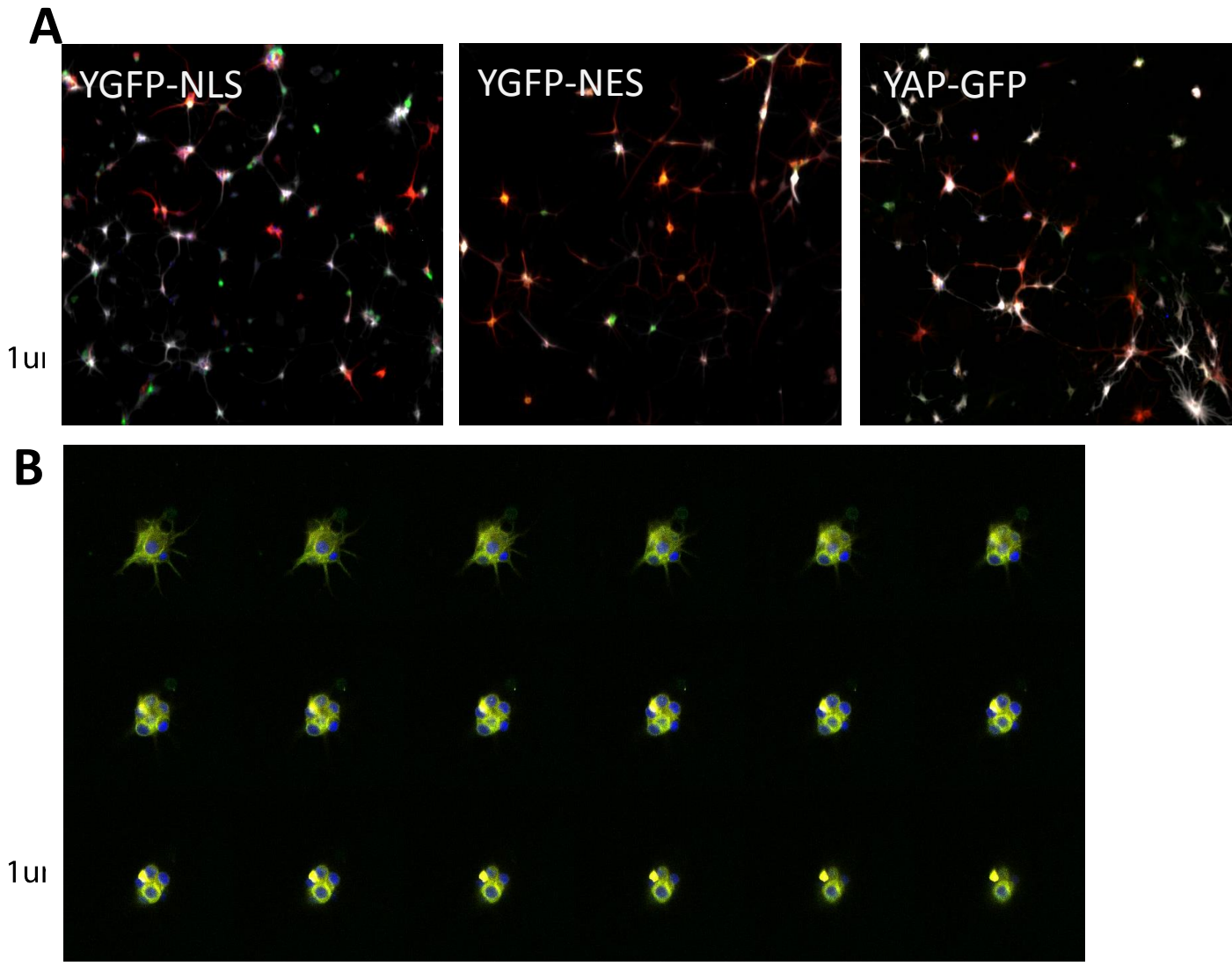
A
YGFP-NLS
YGFP-NES
YAP-GFP
1ul
B
1ul
C
YAP-GFP Differentiation
% Neuronal
% Neuronal
1.0
0.8
0.6
0.4
0.2
0.0
NLS
NES
S94A
VENUS
Infected Construct

Figure 9: Nuclear localization of YAP leads to suppression of neurogenesis, but nuclear export of YAP is enhances neurogenesis on soft substrates. (A): Representative images of (A) YAP-NLS overexpressing NSCs, YAP-NES overexpressing NSCs, and control YAP overexpressing NSCs. (B): Z-stack through YAP-NES overexpressing cells, demonstrating functional nuclear export and cytoplasmic enrichment. (C): Quantification of levels of neurogenesis corresponding to conditions A, B, and S94A and Venus controls.

localization of constructs should not affect the levels of neurogenesis observed. However, we instead found striking differences between the different constructs, with YGFP-NLS cells exhibiting a strong suppression of neurogenesis similar to that of the control construct, but YGFP-NES cells failing to suppress neurogenesis (Fig. 2C). This data suggests that YAP nuclear localization is a key requirement for its ability to suppress β-catenin activity. Though we see no coverall changes in YAP nuclear/cytoplasmic localization on stiff and soft substrates, it may be possible that alternative methods of YAP regulation are controlling its nuclear activity.

For example, YAP phosphorylation may be required to inactivate its β-catenin suppressive ability. If YAP is sequestered to cytoplasm and unable to translocate to nucleus, it may be eventually phosphorylated by canonical Hippo signaling – this seems plausible in differentiating NSCs, as they are post-mitotic cells with potential upregulated LATS1/2 activity. This phosphorylation event may render them unable to bind to β-catenin, and therefore unable to sequester it from binding with transcriptional coactivators and initiating transcription – the serine residue at AA 61 may be a good candidate for this behavior, as it is proximal to a known glutamic acid to alanine mutation that abolishes β-catenin binding[19].

It would be interesting to see if phosphorylation does influence the capability of YAP to transduce mechanical signals or suppress neurogenesis. Studies of phosphorylation and YAP localization have been primarily limited to studies of the primary phosphorylation site by LATS1/2 at serine 127 and rarely linked to mechanosensation. It is possible that any of the other four YAP phosphorylation sites could be responsible for mediating its mechanotrasductive effects. Additionally, even YAP phosphorylated at serine 127 can be found in the nucleus[7] suggesting that nuclear-cytoplasmic partitioning may not be as binary as once considered. These results represent an interesting stepping stone to further unraveling the complex knot of YAP mechanotransduction and its effects on stem cell differentiation.

Works Cited

1. Zhao, B. *et al.* Inactivation of YAP oncoprotein by the Hippo pathway is involved in cell contact inhibition and tissue growth control. *Genes Dev.* 2747–2761 (2007). doi:10.1101/gad.1602907.Hpo/Sav

2. Zhao, B., Li, L., Lei, Q. & Guan, K.-L. The Hippo–YAP pathway in organ size control and tumorigenesis: an updated version. *Genes Dev.* **24,** 862–874 (2010).

3. Zhao, B. *et al.* TEAD mediates YAP-dependent gene induction and growth control TEAD mediates YAP-dependent gene induction and growth control. 1962–1971 (2008). doi:10.1101/gad.1664408

4. Yagi, R., Chen, L. F., Shigesada, K., Murakami, Y. & Ito, Y. A WW domain-containing yes-associated protein (YAP) is a novel transcriptional co-activator. *EMBO J.* **18,** 2551–62 (1999).

5. Lian, I. *et al.* The role of YAP transcription coactivator in regulating stem cell self-renewal and differentiation. *Genes Dev.* **24,** 1106–18 (2010).

6. Dupont, S. *et al.* Role of YAP/TAZ in mechanotransduction. *Nature* **474,** 179–183 (2011).

7. Aragona, M. *et al.* A mechanical checkpoint controls multicellular growth through YAP/TAZ regulation by actin-processing factors. *Cell* **154,** 1047–1059 (2013).

8. Zhao, B. *et al.* Angiomotin is a novel Hippo pathway component that inhibits YAP oncoprotein. *Genes Dev.* **25,** 51–63 (2011).

9. Tumaneng, K. *et al.* YAP mediates crosstalk between the Hippo and PI(3)K–TOR pathways by suppressing PTEN via miR-29. *Nat. Cell Biol.* **14,** 1322–1329 (2012).

10. Park, H. W. *et al.* Alternative Wnt Signaling Activates YAP/TAZ. *Cell* **162,** 780–94 (2015).

11. Azzolin, L. *et al.* YAP/TAZ Incorporation in the β-Catenin Destruction Complex Orchestrates the Wnt Response. *Cell* **158,** 157–170 (2014).

12. Imajo, M., Miyatake, K., Iimura, A., Miyamoto, A. & Nishida, E. A molecular mechanism that links Hippo signalling to the inhibition of Wnt/β-catenin signalling. *EMBO J.* **31,** 1109–22 (2012).

13. Rammensee, S., Kang, M. S., Georgiou, K., Kumar, S. & Schaffer, D. V. Dynamics of Mechanosensitive Neural Stem Cell Differentiation. *Stem Cells* **35,** 497–506 (2017).

14. Lie, D.-C. *et al.* Wnt signalling regulates adult hippocampal neurogenesis. *Nature* **437,** 1370–1375 (2005).

15. Cai, J., Maitra, A., Anders, R. a, Taketo, M. M. & Pan, D. β -Catenin destruction complex- independent regulation of Hippo – YAP signaling by APC in intestinal tumorigenesis. *Genes Dev.* 1–14 (2015). doi:10.1101/gad.264515.115.

16. Konsavage, W. M. & Yochum, G. S. Intersection of Hippo/YAP and Wnt/ -catenin signaling pathways. *Acta Biochim. Biophys. Sin. (Shanghai).* **45,** 71–79 (2013).

17. Saha, K. *et al.* Substrate modulus directs neural stem cell behavior. *Biophys. J.* **95,** 4426–38 (2008).

18. Keung, A. J., de Juan-Pardo, E. M., Schaffer, D. V. & Kumar, S. Rho GTPases Mediate the Mechanosensitive Lineage Commitment of Neural Stem Cells. *Stem Cells* **29,** 1886–1897 (2011).

19. Li, Z. *et al.* Structural insights into the YAP and TEAD complex. *Genes Dev.* **24,** 235–240 (2010).

Chapter 5: Contributions of Hyaluronic Acid Receptor CD44 to Mechanosensitive Neural Stem Cell Differentiation

Jieung, Mike, Kayla

Abstract

In recent years, the impact of matrix properties such as elastic modulus on stem cell differentiation has been a topic of great interest and investigation. However, material limitations have led many in vitro studies to be performed in a two-dimensional experimental system, which loses the influence that a more natural 3-dimensional matrix presentation has on stem cell behavior. Here we describe the ability of 3-dimensional hyaluronic acid hydrogels to strongly upregulate neurogenesis compared to polyacrylamide surfaces, both with and without the presentation of any integrin-binding ligands. We also show that the binding of the surface receptor CD44 to hyaluronic acid is responsible for the observed phenotype, ablation of CD44 expression completely abolished neurogenesis in vitro. These results detail a novel mechanism by which not only matrix properties, but engagement of specific matrix receptors, can have dramatic effects on neuronal fate specification.

Introduction

Adult hippocampal neural stem cells (NSCs) are a class of progenitor cell that resides in the mammalian dentate gyrus, which continually generate new neurons and glia throughout life[1]. This process is controlled by complex, multifactorial set of signals present in the stem cell niche, which can include inputs such as soluble cues[2], neighboring cells[3], extracellular matrix composition[4] and elastic modulus[5–7]. As NSCs are known to contribute to the lifelong processes of learning and memory formation[8] in addition to underlying many disease phenotypes[9], a thorough understanding of the characteristics of the niche is critical for engineering NSCs for therapeutic applications.

In investigating the effects of the properties of the niche on NSC behavior, prior studies have aimed to recreate the niche *in vitro* with varying levels of fidelity. This is complicated by the fact that most *in vitro* systems used to study the brain are stiffer than endogenous brain matrix by a factor of ~10^8. Brain matrix is much softer than other tissues in the body, with bulk spanning a range of 1 - 5 kilopascals[10], and the stem cell niche in the dentate gyrus being softer still, in the range of 80-180Pa[11,12]. The impact of mechanical properties on mesenchymal stem cell behavior has been previously reported[13], and NSCs are similarly influenced by matrix elastic modulus. Previously, our lab used polyacrylamide hydrogels of varying crosslinking density to modulate stiffness, and found that soft matrices enhance neurogenesis, while stiff ones suppress it[5–7]. Additionally, further emulating the natural niche by emulating its dimensionality showed similar impacts on neurogenesis – encapsulation of NSCs in 3-dimensional alginate hydrogels supported neuronal differentiation and maturation, and also showed that stiffer gels suppressed neurogenesis compared to soft ones[14].

However, in addition to substrate stiffness, the extracellular matrix (ECM) of the brain is also unique among organ systems in the body. Relatively sparse in fibrous connective proteins such as fibronectins or collagens[15,16], it is primarily composed of matrix of proteoglycans, in particular tenascin-C, members of the lectican family, and associated glycoasaminoglycans. Primary among these glycosaminogylcans is hyaluronic acid (HA), also known as

hyaluronan[17,18]. HA in the body is non-sulfated, found at high molecular weights (1-10 MDa), extensively remodeled, and rapidly turned over[19]. While the engagement of cells to HA via transmembrane receptors, primarily RHAMM and CD44, has been characterized and implicated in a wide variety of behaviors such as calmodulin-dependent cytoskeletal remodeling[20] and cell migration[21], the influence of HA-binding on NSC proliferation and differentiation has been only recently investigated. Encapsulation of ventral mesencephalic NSCs into a photo-crosslinked hyaluronic acid matrix has shown that an HA-based, stiffness-matched culture system is able to upregulate mature neuronal development[10], and more recently, the digestion of HA in the subgranular zone induces NSC proliferation and delays neuronal differentiation, and stimulation of NSCs with soluble HA induces the complementary phenotype, with robust suppression of proliferation, though without an influence on total neuronal differentiation[4].

Clearly, these reports suggest that the interaction between NSCs and the properties of the niche ECM is a complex and critical process in regulation of adult neurogenesis. However, a study that recapitulates the natural configuration of the niche with respect to stiffness *and* composition in NSCs has not yet been undertaken, largely due to the difficulty of creating reproducible, 3-dimensional culture platforms for *in vitro* experiments. Here, we report the use of a rapid, strain-promoted alkyne addition click chemistry[22] to encapsulate adult hippocampal NSCs into 3-dimensional hyaluronic acid hydrogels. We find that these cells exhibit a degree of stiffness sensitivity, but have a strikingly high level of neurogenesis under all conditions. This phenotype is found to be due to the interactions of hyaluronic acid with CD44, and we highlight a potential downstream signaling pathway that may be implicated in this behavior.

Materials and Methods

Cell Culture

Adult rat NSCs were cultured as previously described in DMEM-F12 (Invitrogen, Carlsbad, California, USA) media with N2 Supplement (Life Technologies, Carlsbad, California, USA), with 20ng/mL FGF-2 (Life Technologies, Carlsbad, California, USA) on tissue-culture polystyrene coated with poly-O-ornithine and laminin. During differentiation, FGF-2 was removed, and the culture was supplemented with mixed differentiation media (1 μg/ml retinoic acid, 1% fetal bovine serum).

Hyaluronic Acid Hydrogels

DBCO-HA hydrogels were synthesized as previously described (Adil, 2017). 1mg of 75kDa molecular weight sodium hyaluronate was reacted with EDC + NHS, and then reacted with 600mg of dibenzocyclooctyne-amine (Sigma) dissolved in DMSO for 3 days. The product was precipitated with cold acetone and spun through a 30kDa cutoff filter. The filtrate was diluted in distilled water, then lyophilized for 3 days to yield a yellow-white product. Reaction yield was characterized by NMR (Supplementary Figure 1).

Crosslinking of hydrogels was conducted by dissolving the lyophilized DBCO-HA in DMEM-F12 at a concentration of 3% by weight, then adding 1100M_n PEG-bisazide (Sigma). Ratios of PEG-bisazide to DBCO-HA is given in Figure 1. These mixtures were then rapidly pipetted into the center of the wells of a superhydrophobic solution-treated 6-well plate, and covered with an air-plasma cleaned 8mm glass coverslip. These were incubated in a humidified incubator at 37°C for 10 minutes. 2mL of DMEM-F12+N2 was added to the well to facilitate

removal of the coverslip, yielding a yielded a cylindrical gel with a height of approximately 100μm, with cells suspended within.

Rheological Characterization

All rheological characterizations were conducted on an Anton-Paar (Ashland, Virginia, USA) Physica MCR301 parallel plate rheometer with an 8mm circular plate geometry. Initial tests were conducted to determine the linear viscoelastic range of the DBCO-HA gels and frequency response – a final value of 0.5% strain and 1Hz frequency was chosen for all data presented. Gels were crosslinked in the rheometer between the plates for maximum contact, and the solvent trap around the plate was filled with water to prevent evaporative drying. Temperature was held constant at 37°C.

Immunocytochemistry

For 3D DBCO-HA gel staining, cells were fixed in 4% paraformaldehyde for 10 minutes, then washed 3 times with PBS for 5 minutes each. Cells were permeabilized and blocked in 5% goat serum and .3% Triton-X 100 at room temperature for 2 hours. Cells were then incubated in with primary antibody in 1% goat serum and .3% Triton-X 100 for 3 days at 4°C to allow for antibody diffusion to reach equilibrium. These samples were then washed in PBS with 1% goat serum and .3% Triton-X 100 3 times, then incubated with secondary antibodies overnight at 4°C. These were then washed once with PBS with 0.3% Triton-X 100 for 15 minutes, then incubated with PBS and 1μg/mL of DAPI for 30 minutes. Cells were washed 2 more times with PBS, then imaged by confocal.

Primary antibodies used were mouse anti-βIII-tubulin (Covance MMS-435P, Princeton, New Jersey, USA) and chicken anti-GFAP (Abcam 7260, Cambridge, UK). Secondary antibodies were purchased from Jackson Labs.

Viral Vector Production

CD44 shRNA was purchased from Dharmacon in the pGIPZ backbone. CD44 CRISPR-Cas9 plasmids were produced using the lentiCRISPRv.2 backbone. PAM sites were identified and selected using Benchling, and six guide sequences were cloned into the plasmid backbone. 293Ts were cultured on a 15cm polystyrene plate in Iscove's Modified Eagle Medium (IMDM) with 10% FBS and 1% penicillin-streptomycin until 90% confluency. 30μg of transfer plasmid, 10μg of psPAX, and 3μg of pMDG.2 were incubated with PEI for 10 minutes in PBS, then dispersed into the plate and swirled. After two and three days, the media was collected and replaced with fresh supplemented IMDM, and purified by ultrafugation through a 20% sucrose gradient.

Antibody Blocking Assay

Antibody blocking to abrogate CD44 engagement was done by incubating resuspended NSCs with a 1:10 solution of anti-CD44 (PA5-21419 Thermo-Fischer) for 15 minutes at 37°C. These cells were then immediately mixed with HA and PEG-bisazide, and allowed to crosslink normally. 2D dimensional experiments with these antibodies were attempted, but discontinued due to low cell engagement.

Results

HA Gel Encapsulation and Survival

We conducted initial experiments to test the reproducibility and dynamic range of our hydrogels. After generating DBCO-functionalized HA (Figure 1A), we characterized the resulting material by 1H-NMR and found approximately 16% functionalization of DBCO to HA. We then crosslinked gels using a variety of molar ratios of PEG-bisazide crosslinker to HA-DBCO (between 0.02:1 and 0.09:1) and measured their shear elastic moduli by parallel plate rheometry. Gels showed rapid crosslinking, reaching equilibrium within 7 minutes and spanning a dynamic range between 100Pa and 1500Pa (Figure 1B). As expected for ~16% functionalization, at ratios higher than 0.08, the stiffness of the gels began to decrease – this corresponds to the formation of singly-attached PEG-bis(azide) crosslinker arms on the HA-DBCO backbone, consuming DBCO groups without creating a crosslink. Additionally, incorporation of a fibronectin-mimetic integrin-binding RGD peptide into the gel using an azido-lysine functionalized peptide showed no significant impact on stiffness up to a 0.04 ratio, corresponding to a stiffness of 1.2kPa. The RGD peptide was chosen due to its ubiquity in other synthesis biomaterial systems[5,23,24] as a translatable integrin-binding motif. In order to maintain parity between the RGD-functionalized and bare HA gels, stiffness values between 100Pa and 1.2kPa were chosen for all 3D encapsulation experiments.

Upon encapsulation of NSCs into these gels, we first analyzed cell survival. On the first day, and after 7 days in culture with FGF-2, we performed a live-dead assay using calcein-AM and ethidium homodimer-1. In both stiff (1.2kPa) and soft (100Pa) gels, there was high viability of >90% in all conditions on day 0 and >80% in all conditions on day 7 (Figure 1C). We also cultured 2D-HA-RGD NSC cultures in parallel, which showed similar levels of viability. . These results demonstrate that long-term cell culture in these materials is feasible and introduces no significant changes to cell viability.

Differentiation of NSCs in 3D-HA-RGD gels

We then assayed differentiation of NSCs in 3D-HA-RGD gels to determine whether creation of a 3D “biomimetic niche” for NSC culture could influence differentiation. We subjected cells to conditions that induce a mixture of neuronal and astrocytic differentiation (i.e. mixed differentiation conditions, 1μM retinoic acid and 1% FBS) and fixed and stained cells for TUJ1 and GFAP expression after a period of 7 days on both 2D-RGD and 3D-HA-RGD gels. Strikingly, all conditions showed a very high level of neurogenesis. Furthermore, while differentiation showed statistically significant differences in differentiation as a function of stiffness, the stiffness sensitivity was modest. That is, all 3D-HA-RGD conditions showed robust neurogenesis in excess of 80% marker positivity, and GFAP+ astrogenesis <10% regardless of substrate stiffness (Figure 1A, B). These levels are significantly higher than the 2D-HA-RGD gels, which showed ~70% TUJ1+ cells on the 100Pa condition, and ~60% at 1.2kPa, and the expected comparison for 2D polyacrylamide surfaces, approximately ~65% at 100Pa and ~35% at 1.2kPa[6].

Unlike polyacrylamide, for the HA gels cells have the potential to choose at least two modes of binding to the material: engagement with integrins via the RGD peptide or with HA via receptors such as CD44. We thus isolated the effects of CD44 binding by creating gels without RGD ("bare" HA) and encapsulated cells within these matrices to determine if they still yielded

high levels of neurogenesis (Figure 3A,B). Interestingly, it appeared that the RGD content had no effect on the level of neurogenesis (Figure 3C), that supplying RGD was dispensable for neurogenesis.

We then assessed whether CD44-binding with HA could be responsible for the high levels of neurogenesis observed. CD44 is a signal to many different downstream signaling partners that include potential neurogenically active pathways. CD44 has been reported and is well known to activate the PI3K/Akt pathway[25], which has been reported to be involved in upregulating neurogenesis[26–28], and has also been reported to attenuate Hippo pathway signaling[29], which our lab has previously identified as critical for stiffness-mediatied neurosuppression. It is also well known as a positive regulator and positive feedback target of Wnt signaling[30], which is known to be a powerful neurogenic signal[31]. We used a CD44-blocking antibody to prevent CD44 engagement with the matrix (Figure 3C) in 3D-HA and found a striking reduction in neurogenesis in both the bare 3D-HA and the 3D-HA-RGD matrix, demonstrating that CD44-HA binding, rather than integrin engagement, apparently mediates HA-driven neurogenesis. Indeed, even the inclusion of integrin binding motifs in the matrix is unable to rescue the sharp reduction in neurogenesis observed. We furthermore asked whether this effect could be replicated with genetic manipulation of CD44, and thus used shRNA to knockdown CD44 and performed the same experiment with similar results (Figure 3D).

Conclusion

Taken together, these results demonstrate that CD44 is a critical component of the NSC response to a hyaluronan network. Previous work in our lab has identified CD44-HA interactions as necessary for glioblastoma cell surface adhesion and spreading[32], and these effects were additive with RGD-binding. We hypothesized initially that the presence of both CD44-HA interactions and integrin-RGD interactions may lead to cytoskeletal changes that bias NSC differentiation towards a neuronal phenotype – but instead, these results suggest that CD44-HA binding alone is sufficient to drive or suppress neurogenesis. Similar results have been reported prior to this study, where CD44 and hyaluronan binding have been recently discovered to also be key regulators of stem cell proliferation and differentation[4]. However, these results are the first to show that modulation of receptor binding or display alone, without disruptions to the bulk matrix or tissue structure, is sufficiently to strongly suppress neurogenesis – even when NSCs are subjected to strong differentiation cues such as retinoic acid and serum. This work represents a novel link in understanding the effects of the matrix composition of the stem cell niche, and lays the foundation for future, investigational studies. It would be of great interest for example to discover which parts of the CD44 signaling molecular, i.e. ERM, akryin, binding – are necessary for neurogenesis. These future projects would lay the ground for precise, highly directed cellular and material engineering to support NSC translational applications.

Figure 1

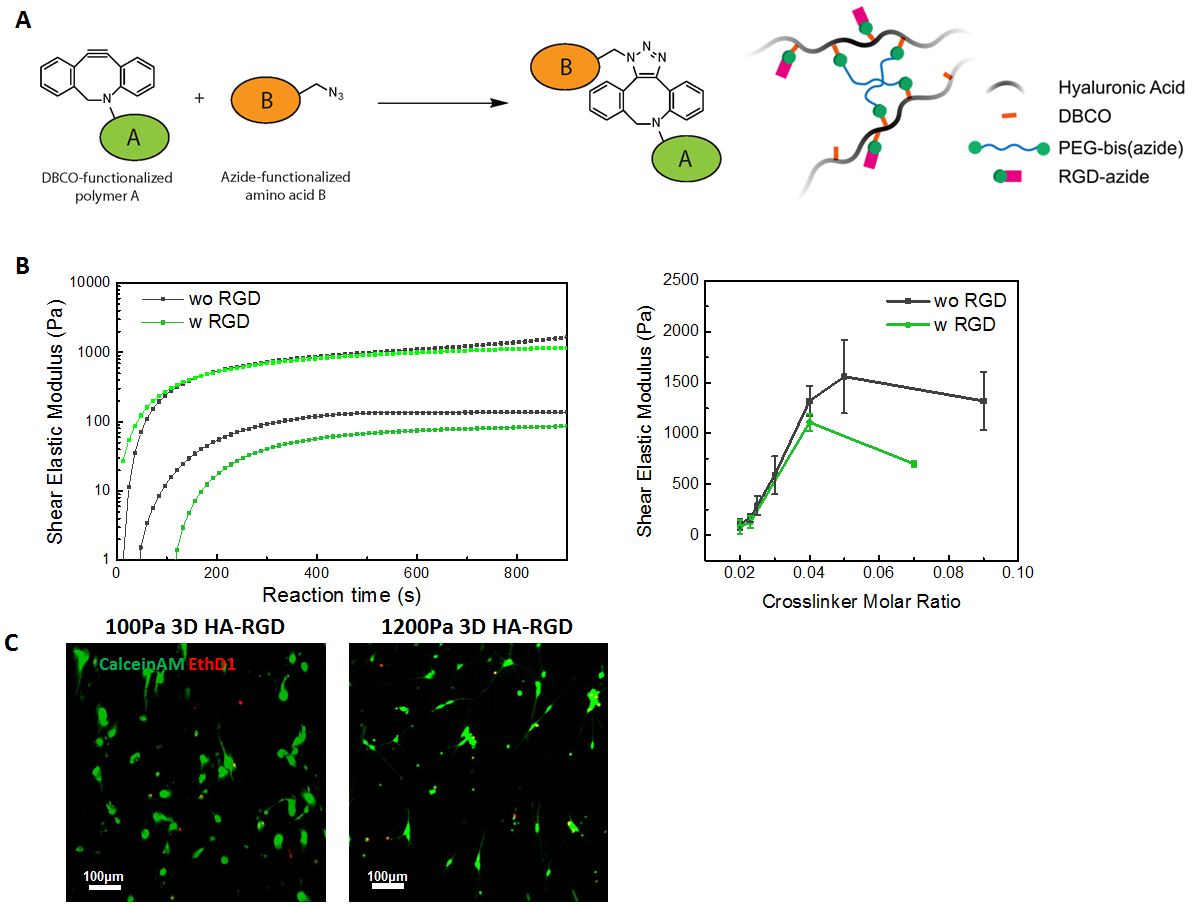

Figure 10: Schematic of hyaluronic acid hydrogels and characterization. (A) Briefly, HA hydrogels were synthesized by a click-chemistry reaction, where dibenzocyclooctyne-functionalized sodium hyaluronate was crosslinked by $\mathbf{PEG}_{\boldsymbol{MN\ 1100}}$ bis-azide by a rapid, strain-promoted alkyne-azide reaction. ECM-mimetic peptide functionality was added into these gels using an azido-modified RGD peptide that was co-crosslinked during gel formation. (B) HA gels showed rapid crosslinking (left) and tunable mechanical properties (right), forming a complete gel within 15 minutes and spanning a dynamic range of 100Pa to 1.2kPa – the slight increase in elastic modulus after 15 min is due to drying of the gel. (C) NSCs encapsulated in these gels showed >80% viability after a period of 7 days in culture by a calcein AM / EthD1 live-dead assay.

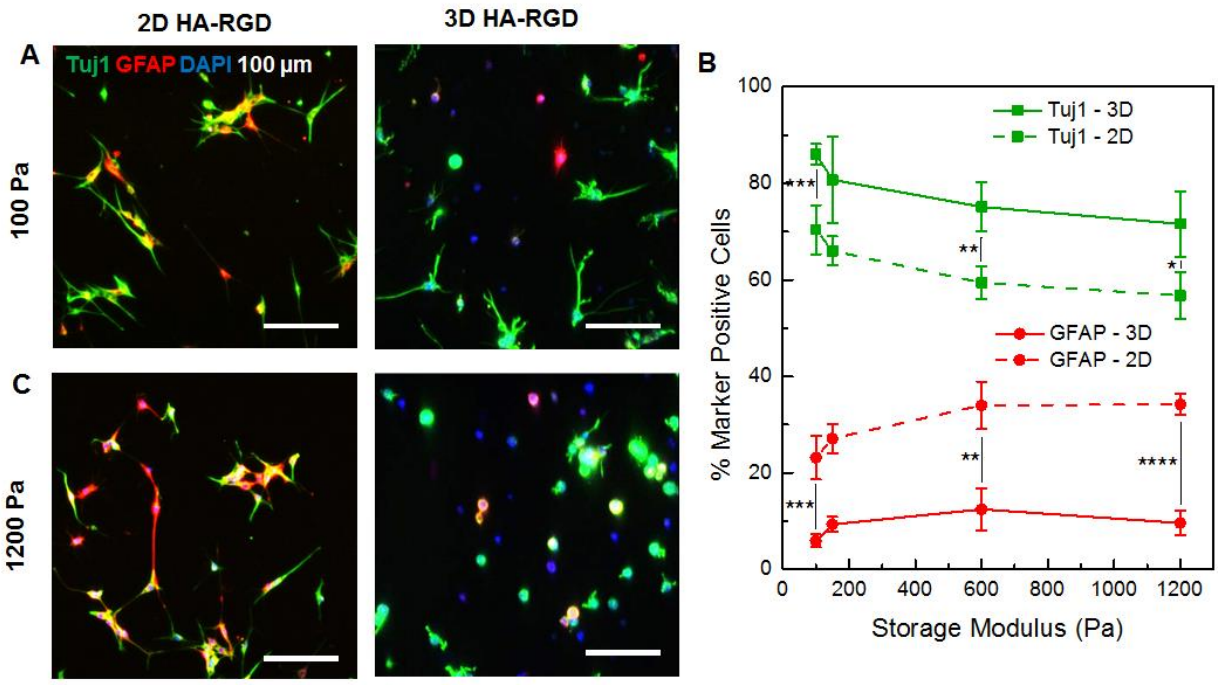

Figure 11: Differentiation of NSCs in 3D HA gels showed robust and consistent neurogenesis, and only slight mechanosensitivity. (A) representative images of NSCs differentiated for 6 days under 1% FBS / 1µM retinoic acid conditions in soft and stiff 3D HA gels with RGD peptide, stained for neuronal markers: DAPI: Blue, βIII-tubulin: Green, GFAP: Red (B) Quantification of differentiation showed that for all conditions, cells were strongly neurogenic, though the stiff condition (1.2kPa) showed a slight reduction in βIII-tubulin positivity, and 2D culture showed a reduction.

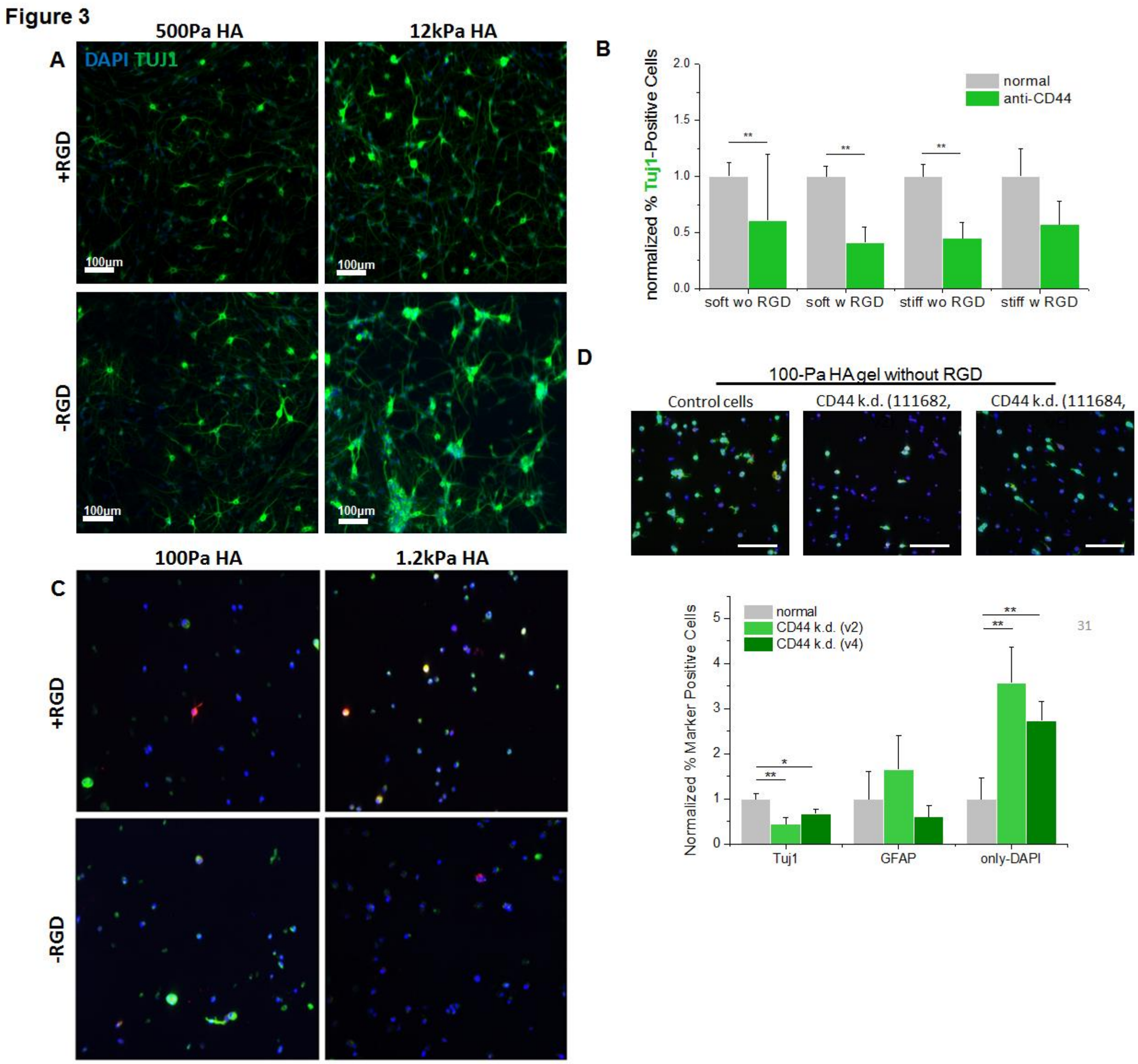

Figure 12: CD44, but not integrin binding, is required for differentiation of NSCs on HA gels. (A) Differentiation of NSCs on bare HA gels with and without RGD both show an elevated, neurogenic phenotype respective to standard plastic or polyacrylamide conditions. (B) Quantification of neurogenesis on bare HA compared to plastic and polyacrylamide of similar stiffness. (C) Inhibition of CD44-HA interactions by incubating NSCs with a CD44 blocking antibody for 30 minutes prior to encapsulation in the gel abolished the neurogenic phenotype dramatically. Repeating this experiment with shRNA knockdown of CD44 yielded similarly striking reductions in neurogenesis.

Works Cited

1. Chen, M.-T. & Weiss, R. Artificial cell-cell communication in yeast Saccharomyces cerevisiae using signaling elements from Arabidopsis thaliana. *Nat. Biotechnol.* **23,** 1551–1555 (2005).

2. Lai, K., Kaspar, B. K., Gage, F. H. & Schaffer, D. V. Sonic hedgehog regulates adult neural progenitor proliferation in vitro and in vivo. *Nat. Neurosci.* **6,** 21–27 (2002).

3. Ashton, R. S. *et al.* Astrocytes regulate adult hippocampal neurogenesis through ephrin-B signaling. *Nat. Neurosci.* **15,** 1399–1406 (2012).

4. Su, W. *et al.* CD44 and hyaluronan regulate neural stem cells CD44 and Hyaluronan Regulate Adult Hippocampal Neural Stem Cell Quiescence and Differentiation. doi:10.1074/jbc.M116.774109

5. Saha, K. *et al.* Substrate modulus directs neural stem cell behavior. *Biophys. J.* **95,** 4426–38 (2008).

6. Keung, A. J., de Juan-Pardo, E. M., Schaffer, D. V. & Kumar, S. Rho GTPases Mediate the Mechanosensitive Lineage Commitment of Neural Stem Cells. *Stem Cells* **29,** 1886–1897 (2011).

7. Rammensee, S., Kang, M. S., Georgiou, K., Kumar, S. & Schaffer, D. V. Dynamics of Mechanosensitive Neural Stem Cell Differentiation. *Stem Cells* **35,** 497–506 (2017).

8. Cao, L. *et al.* VEGF links hippocampal activity with neurogenesis, learning and memory. *Nat. Genet.* **36,** 827–835 (2004).

9. Mu, Y. & Gage, F. H. Adult hippocampal neurogenesis and its role in Alzheimer's disease. *Mol. Neurodegener.* **6,** 85 (2011).

10. Seidlits, S. K. *et al.* The effects of hyaluronic acid hydrogels with tunable mechanical properties on neural progenitor cell differentiation. *Biomaterials* **31,** 3930–3940 (2010).

11. Luque, T., Kang, M. S., Schaffer, D. V & Kumar, S. Microelastic mapping of the rat dentate gyrus. *R. Soc. open Sci.* **3,** 150702 (2016).

12. Elkin, B. S., Azeloglu, E. U., Costa, K. D. & Morrison III, B. Mechanical Heterogeneity of the Rat Hippocampus Measured by Atomic Force Microscope Indentation. *J. Neurotrauma* **24,** 812–822 (2007).

13. Engler, A. J., Sen, S., Sweeney, H. L. & Discher, D. E. Matrix Elasticity Directs Stem Cell Lineage Specification. *Cell* **126,** 677–689 (2006).

14. Banerjee, A. *et al.* The influence of hydrogel modulus on the proliferation and differentiation of encapsulated neural stem cells. *Biomaterials* **30,** 4695–4699 (2009).

15. Ruoslahti, E. Brain extracellular matrix. *Glycobiology* **6,** 489–92 (1996).

16. Rauch, U. Brain matrix: structure, turnover and necessity. *Biochem. Soc. Trans.* **35,** 656–660 (2007).

17. Bignami, A., Hosley, M. & Dahl, D. Hyaluronic acid and hyaluronic acid-binding proteins in brain extracellular matrix. *Anat. Embryol. (Berl).* **188,** 419–33 (1993).

18. Toole, B. P. Hyaluronan: from extracellular glue to pericellular cue. *Nat. Rev. Cancer* **4,** 528–539 (2004).

19. Whitesides, G. M. Whitesides' Group: Writing a Paper. *Adv. Mater.* **16,** 1375–1377 (2004).

20. Lynn, B. D., Turley, E. A. & Nagy, J. I. Subcellular distribution, calmodulin interaction, and mitochondrial association of the hyaluronan-binding protein RHAMM in rat brain. *J. Neurosci. Res.* **65,** 6–16 (2001).

21. Casini, P., Nardi, I. & Ori, M. RHAMM mRNA expression in proliferating and migrating cells of the developing central nervous system. *Gene Expr. Patterns* **10,** 93–97 (2010).

22. Adil, M. M. *et al.* Engineered hydrogels increase the post-transplantation survival of encapsulated hESC-derived midbrain dopaminergic neurons. *Biomaterials* **136,** 1–11 (2017).

23. Maheshwari, G., Brown, G., Lauffenburger, D. A., Wells, A. & Griffith, L. G. Cell adhesion and motility depend on nanoscale RGD clustering. *J. Cell Sci.* **113 (Pt 10),** 1677–86 (2000).

24. Reinhart-King, C. A., Dembo, M. & Hammer, D. A. Cell-cell mechanical communication through compliant substrates. *Biophys. J.* **95,** 6044–51 (2008).

25. Lin, Y. H. & Yang-Yen, H. F. The Osteopontin-CD44 Survival Signal Involves Activation of the Phosphatidylinositol 3-Kinase/Akt Signaling Pathway. *J. Biol. Chem.* **276,** 46024–46030 (2001).

26. Peltier, J., O'Neill, A. & Schaffer, D. V. PI3K/Akt and CREB regulate adult neural hippocampal progenitor proliferation and differentiation. *Dev. Neurobiol.* **67,** 1348–1361 (2007).

27. Shioda, N., Han, F. & Fukunaga, K. in *International review of neurobiology* **85,** 375–387 (2009).

28. Bruel-Jungerman, E. *et al.* Inhibition of PI3K-Akt Signaling Blocks Exercise-Mediated Enhancement of Adult Neurogenesis and Synaptic Plasticity in the Dentate Gyrus. *PLoS One* **4,** e7901 (2009).

29. Xu, Y., Stamenkovic, I. & Yu, Q. CD44 attenuates activation of the Hippo signaling pathway and is a prime therapeutic target for glioblastoma. *Cancer Res.* **70,** 2455–2464 (2010).

30. Schmitt, M., Metzger, M., Gradl, D., Davidson, G. & Orian-Rousseau, V. CD44 functions in Wnt signaling by regulating LRP6 localization and activation. *Cell Death Differ.* **22,** 677–689 (2015).

31. Lie, D.-C. *et al.* Wnt signalling regulates adult hippocampal neurogenesis. *Nature* **437,** 1370–1375 (2005).

32. Kim, Y. & Kumar, S. CD44-mediated adhesion to hyaluronic acid contributes to mechanosensing and invasive motility. *Mol. Cancer Res.* **12,** 1416–29 (2014).

Chapter 6: Conclusions

The work presented in this dissertation explores the mechanical identity of the adult mammalian NSC niche, and examines both the essential properties of the endogenous tissue and engineers new material systems to better recapitulate those findings. In Chapter 1, we provided a perspective on the complexity of the NSC niche, the variety of networked and interconnected signaling pathways that connect and unify NSC behavior and biology, and the place of mechanical stimuli within that network. Many previously identified signaling pathways are not merely orthogonal to biomechanics, but instead synergize with or antagonize their effects, leading to a complicated web – a small part of which is illuminated by this work.

In Chapter 2, we began with a micromechanical study of the NSC niche in the adult rat hippocampus. As NSCs have been previously reported as mechanosensitive, we were interested in discovering whether endogenous mechanical patterns or heterogeneities may exist that could inform future platform design and studies. We found that the niche is highly heterogeneous, spanning a ~3fold range of stiffnesses within the subgranular zone and the granule cell layer, and hypothesize that this patterning may influence the timing of signals reaching NSCs, or may guide their migration during maturation. We chose the former of these hypothesizes to investigate further in Chapter 3.

Here, we used our understanding of the basic mechanical properties of the brain in order to design a dynamic hydrogel that allows us to modulate the stiffness environment presented to NSCs in a temporally defined fashion. We found that NSCs show mechanosensitivity only during a particular window during differentiation, and that the messenger of these effects is the transcriptional coactivator YAP. We proceed with further biomolecular studies of YAP activity, and find that it strongly suppresses β-catenin transcriptional activation and appears to mediate neurosuppression in a TEAD-independent manner. We further the depth of these studies in Chapter 4, where we investigate the specific requirements of YAP localization for its effects on β-catenin activation, and discover that there is a strong, *nuclear* requirement for YAP to suppress β-catenin. This is at odds with previously proposed models of the YAP-β-catenin interaction, and we have laid the groundwork for further investigation into this interaction.

In Chapter 5, we take a step back and return to recapitulating the brain environment, but from the perspective of dimensionality and composition. We find that 3D hyaluronan encapsulation of NSCs leads to very robust neuronal differentiation compared to 2D or polyacrylamide surfaces. Interestingly, we find that addition of RGD into these gels is dispensable for neurogenesis, and with further inquiry have revealed the cell-surface glycoprotein CD44 as responsible and necessary for mediating HA-directed neurogenesis.

Taken together, these studies have tackled the fundamental question of "how does the NSC niche support differentiation into mature neurons?" The answer to this question is a multi-faceted, highly complex network of coordinated, interconnecting signaling pathways and molecules – however, discovering how neurogenesis occurs in the brain is an important fundamental challenge in learning how to engineer NSCs for therapeutic benefit or for understanding the foundations of neurological disease.